

**The IPAC-NC field  
campaign**

J. Z. Ma et al.

This discussion paper is/has been under review for the journal Atmospheric Chemistry and Physics (ACP). Please refer to the corresponding final paper in ACP if available.

# The IPAC-NC field campaign: a pollution and oxidization pool in the lower atmosphere over Huabei, China

J. Z. Ma<sup>1</sup>, W. Wang<sup>2,†</sup>, Y. Chen<sup>1</sup>, H. J. Liu<sup>2</sup>, P. Yan<sup>1</sup>, G. A. Ding<sup>1</sup>, M. L. Wang<sup>1</sup>, and J. Lelieveld<sup>3,4,5</sup>

<sup>1</sup>Chinese Academy of Meteorological Sciences, Beijing, China

<sup>2</sup>Chinese Research Academy of Environmental Sciences, Beijing, China

<sup>3</sup>Max Planck Institute for Chemistry, Mainz, Germany

<sup>4</sup>Cyprus Institute, Nicosia, Cyprus

<sup>5</sup>King Saud University, Riyadh, Saudi Arabia

<sup>†</sup>deceased, March 2010

Received: 5 September 2011 – Accepted: 3 October 2011 – Published: 12 October 2011

Correspondence to: J. Z. Ma (mjz@cams.cma.gov.cn)

Published by Copernicus Publications on behalf of the European Geosciences Union.

Title Page

Abstract

Introduction

Conclusions

References

Tables

Figures

◀

▶

◀

▶

Back

Close

Full Screen / Esc

Printer-friendly Version

Interactive Discussion



## Abstract

In the past decades, regional air pollution characterized by photochemical smog and grey haze-fog has become a severe environmental problem in China. To investigate this, a field measurement campaign was performed in the Huabei region, located between 32°–42° N latitude in Eastern China, during the period 2 April–16 May 2006 as part of the project “Influence of Pollution on Aerosols and Cloud Microphysics in North China” (IPAC-NC). It was found that strong pollution emissions from urban and industrial centers accumulate in the lower atmosphere over the core area of Huabei. We observed widespread, very high SO<sub>2</sub> mixing ratios, about 20–40 ppbv at 0.5–1.5 km altitude and 10–30 ppbv at 1.5–3.0 km altitude. Average CO mixing ratios were 0.65–0.7 ppmv at 0.5–1.5 km altitude, and very high CO around 1 ppmv was observed during some flights, and even higher levels at the surface. The high pollution concentrations were associated with enhanced levels of OH and HO<sub>2</sub> radicals, calculated with a chemical box model constrained by the measurements. The maximum OH concentration was  $6.9 \times 10^6$  molecules cm<sup>-3</sup> (~0.29 pptv) at an altitude of ~1 km, remarkably higher than  $5.4 \times 10^6$  molecules cm<sup>-3</sup> (~0.22 pptv) at the surface. In the upper part of the boundary layer and in the lower free troposphere, high CO and SO<sub>2</sub> competed with relatively less NO<sub>2</sub> in reacting with OH, being efficiently recycled through HO<sub>2</sub>, preventing a net loss of HO<sub>x</sub> radicals. In addition to reactive hydrocarbons and CO, the oxidation of SO<sub>2</sub> caused significant ozone production over Huabei (up to ~13 % or 2.0 ppbv h<sup>-1</sup> at ~0.8 km). The enhanced OH increased the formation of condensable species by the oxidation of volatile precursor gases, adding to the high loadings of mineral dust particles. Our results indicate that the lower atmosphere over Huabei is not only strongly polluted but also acts as an oxidation pool over Eastern China.

## The IPAC-NC field campaign

J. Z. Ma et al.

Title Page

Abstract

Introduction

Conclusions

References

Tables

Figures

◀

▶

◀

▶

Back

Close

Full Screen / Esc

Printer-friendly Version

Interactive Discussion



## 1 Introduction

The growing influence of gas and aerosol emissions from major urban and industrial centers on air quality and climate on regional to global scales is of great concern. In recent decades, intensive field campaigns and model studies have demonstrated that global air pollution is strongly affected by regional hot spots of air pollution (Lelieveld et al., 2002a; Akimoto, 2003; Lawrence et al., 2007). These hot spot regions of severe air pollution often include megacities (>10 million population) with strongly enhanced emissions from traffic, power generation and industrial activities (Molina and Molina, 2004; Gurjar et al., 2008). While urban and regional pollution in the traditional industrialized countries continues to provide environmental challenges, the attention for developing and newly industrialized regions, e.g., in Middle America (Molina et al., 2007, 2010), the Mediterranean (Kanakidou et al., 2011), Middle East (Lelieveld et al., 2009) and South and East Asia (Chan and Yao, 2008; Zhang et al., 2008c; Lawrence and Lelieveld, 2010; Ma et al., 2010) is intensifying.

Photochemical smog has become a major concern in the urban environment (Molina and Molina, 2004). Emissions of nitrogen oxides ( $\text{NO}_x \equiv \text{NO} + \text{NO}_2$ ), carbon monoxide (CO) and volatile organic compounds (VOCs) drive the photochemical formation of ozone ( $\text{O}_3$ ) and other oxidants, degrading air quality and adversely affecting human health, ecosystems and agricultural productivity (Molina et al., 2010). Atmospheric ozone production,  $\text{P}(\text{O}_3)$ , over urban centers generally involves different stages, from being VOC-sensitive near the source(s) to being rather more  $\text{NO}_x$ -sensitive further downwind (Sillman, 1999; Solomon et al., 2000; Kleinman et al., 2005; Kuhn et al., 2010). Photochemical smog episodes are accompanied by high aerosol loads, causing haze pollution with potential impacts on human health, climate and the hydrological cycle (Ramanathan et al., 2005; Pope and Dockery, 2006; Ma et al., 2010). These aerosols, mainly consisting of fine particles, originate either directly from traffic, industrial activity and biomass burning (primary particles), or indirectly from the gas-to-particle conversion of low-volatile condensable inorganic and organic

### The IPAC-NC field campaign

J. Z. Ma et al.

Title Page

Abstract

Introduction

Conclusions

References

Tables

Figures

◀

▶

◀

▶

Back

Close

Full Screen / Esc

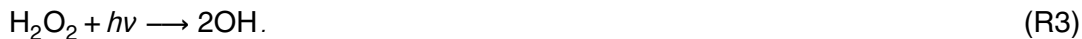
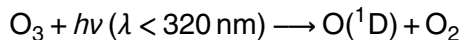
Printer-friendly Version

Interactive Discussion



gases (secondary particles), formed via a complex sequence of oxidation reactions of gaseous precursors from the same sources (Seinfeld and Pandis, 1998; Kulmala, 2003; Jimenez et al., 2009; Apel et al., 2010).

5 The oxidation of gaseous precursors of ozone and secondary aerosols is mainly initiated by hydroxyl radicals (OH), formed primarily through the photolysis of O<sub>3</sub>, nitrous acid (HNO<sub>2</sub>), and hydrogen peroxide (H<sub>2</sub>O<sub>2</sub>) (Levy, 1971; Ehhalt, 1999).



The reactions of OH with CO and VOCs (expressed as RH in Eq. (R5)) produce hydroperoxy (HO<sub>2</sub>) and organic peroxy (RO<sub>2</sub>) radicals, respectively.



RO<sub>2</sub> (expressed as R'CH<sub>2</sub>O<sub>2</sub> in Eq. (R6)) is converted to HO<sub>2</sub> through reaction with NO. HO<sub>2</sub> further reacts with NO to recycle OH.



NO<sub>2</sub> produces O<sub>3</sub> and reforms NO upon photolysis by sunlight.

**The IPAC-NC field campaign**

J. Z. Ma et al.

Title Page

Abstract

Introduction

Conclusions

References

Tables

Figures

I◀

▶I

◀

▶

Back

Close

Full Screen / Esc

Printer-friendly Version

Interactive Discussion



In addition to the effective photodissociation of ozone Eq. (R1), ozone loss occurs through the  $\text{HO}_x$  ( $\equiv \text{OH} + \text{HO}_2$ ) catalytic cycle and addition reaction with alkenes.



Loss of OH occurs through the reaction with  $\text{NO}_2$ , forming nitric acid ( $\text{HNO}_3$ ).



$\text{O}_3$  production through the catalytic cycle between NO and  $\text{NO}_2$  is thus associated with the competition for OH radicals by CO, VOCs and  $\text{NO}_x$ , and a potential recycling between OH and  $\text{HO}_2$  (Kuhn et al., 2010). Additional OH results from the photolysis of  $\text{O}_3$  and can be amplified in the oxidation of VOCs, but the chemical mechanisms have not yet been fully understood (Lelieveld et al., 2008; Hofzumahaus et al., 2009). How OH recycling may enhance the efficiency of atmospheric oxidation processes on urban to global scales needs further investigation of the organic radical chemistry, though empirical  $\text{HO}_x$  budget studies have recently been reported, e.g., for Mexico City (Volkamer et al., 2010; Sheehy et al., 2010), for the rural area in the Pear River Delta, China (Lou et al., 2010), for the boundary layer and free troposphere (FT) over West Africa (Commane et al., 2010), for the tropical troposphere over the Amazon rainforest (Martinez et al., 2010; Kubistin et al., 2010), and for the Arctic troposphere (Mao et al., 2010; Lelieveld, 2010).

Regional air pollution characterized by photochemical smog and haze-fog has been recognized as one of the severe environmental problems in China (Zhang et al., 2008c; Ma et al., 2010). North China, or Huabei in Chinese (hereafter we use the latter), is a geographical region located between  $32^\circ$ – $42^\circ$  N latitude in the northern part of Eastern China, including several provinces and large municipalities, e.g., Beijing and Tianjin. Over the past decades, the region has actually become one of the most severely

## The IPAC-NC field campaign

J. Z. Ma et al.

Title Page

Abstract

Introduction

Conclusions

References

Tables

Figures

◀

▶

◀

▶

Back

Close

Full Screen / Esc

Printer-friendly Version

Interactive Discussion





high concentrations of gaseous pollutants and aerosol particles mixed within low-level stratiform clouds (Ma et al., 2010). IPAC-NC also revealed that oxidation reactions associated with high OH play a central role in the formation and persistence of the haze-clouds (Ma et al., 2010). Here we analyze the data with a focus on trace gases, ozone photochemistry and the atmospheric oxidation capacity.

## 2 IPAC-NC field experiment

### 2.1 Emissions and meteorology

The IPAC-NC campaign was performed in the larger Beijing, Tianjin, and Tangshan area (called Jing-Jin-Tang in Chinese) with some flight tracks extending towards the Bohai Gulf. The research area was strongly influenced by air pollution emissions and transport from major urban and industrial centers in the region of Huabei. According to an emission inventory for Huabei developed by our group (Zhao et al., 2011), anthropogenic emissions in the core area, i.e., the Beijing Municipality, Tianjin Municipality and Hebei Province (together forming Jing-Jin-Ji) in the year 2003 were: 2.06 Tg SO<sub>2</sub>, 1.58 Tg NO<sub>x</sub> (in equivalent NO<sub>2</sub>), 1.32 Tg VOC, 16.11 Tg CO, 1.19 Tg NH<sub>3</sub>, 2.65 Tg PM<sub>10</sub>, 1.40 Tg PM<sub>2.5</sub>, 0.11 Tg EC, and 0.25 Tg OC. Figure 1 presents the spatial distributions of emission sources of primary air pollutants in Jing-Jin-Ji. The large emission centers coincide with megacities (Beijing 39.92° N, 116.46° E and Tianjin 39.02° N, 117.02° E) and other large industrial cities (Tangshan 39.36° N, 118.11° E, Shijiazhuang 38.02° N, 114.30° E). While Jing-Jin-Ji is one of the major industrial areas in China, Shanxi Province in West Huabei (not shown in the figure) is important for its energy production, with large pollution sources (e.g., Taiyuan City 37.54° N, 112.33° E), included in our database.

The IPAC-NC campaign was carried out in spring 2006. During this season warm and humid southerly and southwesterly winds prevail in the planetary boundary layer, often invaded by northwesterly cold, dry air masses. Above the boundary layer, westerly and northwesterly winds prevail. In addition to the synoptic weather systems,

## The IPAC-NC field campaign

J. Z. Ma et al.

Title Page

Abstract

Introduction

Conclusions

References

Tables

Figures

◀

▶

◀

▶

Back

Close

Full Screen / Esc

Printer-friendly Version

Interactive Discussion



**The IPAC-NC field campaign**

J. Z. Ma et al.

Title Page

Abstract

Introduction

Conclusions

References

Tables

Figures

◀

▶

◀

▶

Back

Close

Full Screen / Esc

Printer-friendly Version

Interactive Discussion



the circulation pattern is influenced by the pronounced topography in the north and west of the Jing-Jin-Tang area (Xu et al., 2005; Chen et al., 2009). We added passive pollution tracers into the regional meteorological forecast model GRAPES to simulate the transport of pollutants from the large cities Beijing, Tianjin, Tangshan, Shijiazhuang, and Taiyuan, respectively. The tracers were released from the five  $0.3^\circ \times 0.3^\circ$  model grids for each city in the lowest model layer. A constant tracer emission rate of  $300 \text{ Mg km}^{-2}$  was used for all selected grid cells, comparable to the  $\text{SO}_2$  and  $\text{NO}_x$  emissions in these cities. Figure 2 shows the wind fields and spatial tracer distributions over Jing-Jin-Tang and the surrounding areas during the campaign period. In addition to the concentrated pollution hot spots near the ground, strongly enhanced tracer concentrations are predicted at higher altitudes up to  $\sim 3 \text{ km}$ . The weak vertical winds and horizontal convergence lead to the accumulation of pollutants, thus resulting in an “air pollution pool” over the area.

## 2.2 Satellite data and model analysis

Satellite data of tropospheric  $\text{NO}_2$  vertical column densities (VCDs) have been widely used to identify pollution hot spots and emission changes worldwide, since  $\text{NO}_2$  has a short lifetime (about one day) and the data retrieval products are relatively robust (Richter et al., 2005; Ma et al., 2006; Wang et al., 2007; Zhang et al., 2008b; Lelieveld et al., 2009; Mijling et al., 2009; Yu et al., 2010). Ozone Monitoring Instrument (OMI) satellite data of tropospheric  $\text{NO}_2$  VCDs, retrieved by KNMI/NASA at a resolution of  $0.15^\circ \times 0.15^\circ$  (Boersma et al., 2007), are available through the internet (<http://www.temis.nl>). Figure 3a shows OMI tropospheric  $\text{NO}_2$  VCDs over the central area of Huabei during IPAC-NC. Maximum  $\text{NO}_2$  VCDs are found to be  $2 \times 10^{16}$ – $3 \times 10^{16}$  molecules  $\text{cm}^{-2}$  over the urban centers of Beijing and Shijiazhuang. In the larger Jing-Jin-Tang and Shijiazhuang areas, the  $\text{NO}_2$  VCDs are higher than  $1 \times 10^{16}$  molecules  $\text{cm}^{-2}$ , comparable to the levels over some urban centers in other regions of the world (Boersma et al., 2008), indicating widespread pollution over the region.

**The IPAC-NC field campaign**

J. Z. Ma et al.

Title Page

Abstract

Introduction

Conclusions

References

Tables

Figures

◀

▶

◀

▶

Back

Close

Full Screen / Esc

Printer-friendly Version

Interactive Discussion



We calculated tropospheric NO<sub>2</sub> vertical column densities using our regional chemical transport model (RCTM) (Ma et al., 2002a) with an updated high-resolution (10 km × 10 km) emission inventory for the year 2003 developed by Zhao et al. (2011) and the chemical lateral boundary conditions from the EMAC global model (Jöckel et al., 2006); and the results are presented in Fig. 3b. The NO<sub>2</sub> pollution hot spots of Beijing, Tianjin, Tangshan, and Shijiazhuang are clearly shown by both OMI and our RCTM simulation. It is noted that there are some disagreements between the satellite data and model results in the absolute NO<sub>2</sub> column values. The reason may be uncertainties both in satellite products and model simulations, the latter probably related to emission uncertainties. To investigate this we performed a sensitivity simulation in which industrial NO<sub>x</sub> emissions were doubled throughout the domain. The results from this simulation indicate a strong overestimation of the NO<sub>2</sub> columns over urban centers such as Beijing, while NO<sub>2</sub> columns in the surrounding regions are still too low. It thus appears that the major urban-industrial NO<sub>x</sub> sources are reasonably well represented in our emission database. Rural emissions, on the other hand, possibly from small scale industrial and agricultural activities, i.e. more difficult to capture by statistical datasets, are probably underestimated.

We also used a tracer-tagging method implemented in our RCTM, as described by Ma et al. (2002c), to simulate transport and transformation of nitrogen compounds originating from different emission sources. Figure 3c presents the percentage contributions of industrial, traffic, and other sources to tropospheric NO<sub>2</sub> vertical column densities in the central area of Huabei. The other sources refer to the emissions from civil activities and biomass burning and the inflow from outside of the Huabei model domain. Interestingly, the pollution characteristics in different areas of Huabei are quite different. For example, the atmospheres over the Beijing and Shijiazhuang areas are influenced predominantly by traffic emissions (~50–70 %) and the atmospheres over Tianjin and Tangshan by industrial pollution (~60–80 %). Note that this result may not apply to urban air quality at the surface where traffic emissions generally dominate the pollution sources.

## 2.3 Measurement platforms and instruments

The principal measurement platforms of IPAC-NC included a twin-engine YUN-12 aircraft operated from Tianjin International Airport and two ground stations, one located at 39.88° N, 116.47° E on the campus of the Beijing University of Technology (Beigongda station), and the other at 39.73° N, 117.53° E in the Xin'an weather modification station of the Baodi County of Tianjin Municipality (Xin'an station, previously referred as Baodi station by Ma et al., 2010). Beigongda is an urban site in the southeast of Beijing, about 1 km away (inside) from the East 4th Ring Road, and the instruments were located on the roof of an 11-story building. Xin'an is a rural site in the center of Jing-Jin-Tang, about 85 km, 70 km, and 105 km away from Beijing, Tianjin, and Tangshan, respectively, and the instruments were located on the roof of a single-story building. The Xi'an site is surrounded by agricultural fields, about 1 km from the small town. Trace gases (including SO<sub>2</sub>, NO<sub>x</sub>, CO, VOCs, and O<sub>3</sub>) and aerosols (mass and chemical composition of PM<sub>2.5</sub>) were measured at the two stations. In addition, the particle size distributions and the aerosol scattering coefficients as a function of relative humidity were measured at the Xin'an site (Pan et al., 2009; Ma et al., 2010).

Table 2 gives a summary of the instruments mounted on board the aircraft to measure trace gases, aerosols, clouds, and meteorological parameters (Wang et al., 2008; Ma et al., 2010). A FEP-Teflon tube was used to introduce the ambient air from below the fuselage into the aircraft cabin for gas analysis. O<sub>3</sub> was measured by a UV-absorption analyzer (TECO Model 49, USA) with a response time of 20 s. Nitrogen oxides were monitored by an O<sub>3</sub>-chemiluminescence NO-NO<sub>x</sub> analyzer (TECO Model 42C-TI, USA) with a response time of 10 s. The reactive nitrogen species detected as NO<sub>x</sub> with this analyzer probably include some NO<sub>y</sub> (e.g., nitric acid and organic nitrates) and will be denoted as NO<sub>x</sub>\* following Hatakeyama et al. (2005). SO<sub>2</sub> was monitored by a UV pulse fluorescence analyzer (TECO Model 43C-TL, USA) with a response time of about 80 s. CO was monitored by a gas filter correlation analyzer (TECO Model 48C, USA) with a response time of about 1 s. All instruments were aligned with zero air

### The IPAC-NC field campaign

J. Z. Ma et al.

[Title Page](#)[Abstract](#)[Introduction](#)[Conclusions](#)[References](#)[Tables](#)[Figures](#)[◀](#)[▶](#)[◀](#)[▶](#)[Back](#)[Close](#)[Full Screen / Esc](#)[Printer-friendly Version](#)[Interactive Discussion](#)

---

**The IPAC-NC field campaign**J. Z. Ma et al.

---

[Title Page](#)[Abstract](#)[Introduction](#)[Conclusions](#)[References](#)[Tables](#)[Figures](#)[◀](#)[▶](#)[◀](#)[▶](#)[Back](#)[Close](#)[Full Screen / Esc](#)[Printer-friendly Version](#)[Interactive Discussion](#)

before and after entering the sampling areas during every flight. Since the CO analyzer on board the aircraft needed a relatively long period for stabilization during each flight, only the second half of the CO data could be used for analyses. The chemistry instruments on board the aircraft were turned on about 15 min after taking off and switched off about 15 min before landing. VOCs sampling was done using 2–4 canisters each flight and were typically filled during 10–20 min per canister. After the flight, the samplers were directly sent to the State Joint Key Laboratory of Environmental Simulation and Pollution at Peking University for chemical analyses (Shao et al., 2009).

Ground and aircraft aerosol filter sampling as well as the chemical analyses were conducted using the methods as described in previous studies (Pan et al., 2009; Ma et al., 2010). Condensation nuclei (CN) concentrations were measured at a frequency of 1 Hz with a condensation particle counter (TSI-3020, USA) which detects submicrometer particles larger than 5 nm diameter. Ultrafine particle concentrations with diameters of 5.6–560 nm were measured with an Engine Exhaust Particle Sizer Spectrometer (EEPS) model 3090 (TSI-3090, USA) at 1 Hz frequency. A diversion dome was mounted on the belly of the fuselage to introduce ambient air into the sampling tubes and the sample air was introduced into the aircraft cabin through stainless steel and conductive carbon tubes. The sampling flow rates were  $2\text{ l min}^{-1}$  for CN and  $10\text{ l min}^{-1}$  for the EEPS. Accumulation mode aerosols of 0.1–3.0  $\mu\text{m}$  diameter were measured with a Particle Cavity Aerosol Spectrometer Probe (PCASP-100X, PMS, USA), and cloud droplet number concentrations of 2–47  $\mu\text{m}$  diameter were determined using a Forward Scattering Spectrometer Probe (FSSP-100, PMS, USA). These two PMS probes were installed externally on the belly of the aircraft to measure the particle and droplet size distribution at ambient humidity. Temperature, relative humidity, and geographical information (latitude, longitude, and altitude) were measured continuously with a thermometer (EMM-01), a dew-point hydrometer (DP3-D-SH, Tempcontrol, NL), and a global positioning system (GPS, Global Water, USA). Detailed descriptions of the instruments and aircraft sampling system can be found in Wang et al. (2008) and Ma et al. (2010).

## 2.4 Aircraft flight time and areas

Table 3 presents an overview of the flights performed in IPAC-NC. The aircraft transferred from the Changzhou city of Jiangsu Province in Southern China to the Tianjin airport on 2 April 2006, and back to Changzhou on 16 May 2006. Most instruments were on board during the transfer flights (TF), and thus the measurement data obtained over the Huabei region on these two days can also be used for this study. Seventeen research flights (RF) were performed during the campaign, including eight under clear-sky conditions (described as hazy for some days), eight under cloudy conditions, and one during a dust storm (RF06). Several flight patterns were designed and implemented based on a combination of research objectives, weather conditions, and air traffic control regulations. The flight altitude ranged up to 3500 m the cruising velocity was generally  $\sim 200 \text{ km h}^{-1}$ , and the flight duration was typically around 4–5 h. Figure 4 shows all flight tracks individually, and Fig. 5 presents their spatial coverage by combining all research flight tracks in one overview. The aircraft measurements took place over the Tianjin and Tangshan areas and the downwind region, located within the above described air pollution pool.

## 3 Results and discussion

Here we present our analytical results including statistics and model calculations based on the data obtained during the campaign, focusing on the general chemical characteristics over the region. Detailed episode analyses, e.g., the influence of local meteorological conditions on the measurement results, will be presented in dedicated papers.

### The IPAC-NC field campaign

J. Z. Ma et al.

Title Page

Abstract

Introduction

Conclusions

References

Tables

Figures

◀

▶

◀

▶

Back

Close

Full Screen / Esc

Printer-friendly Version

Interactive Discussion



### 3.1 Urban and regional pollution observed on the ground

Figure 6 shows average diurnal variations of trace gases measured at the Beigongda (urban) and Xin'an (rural) stations. High concentrations of primary pollutants  $\text{SO}_2$ ,  $\text{NO}$ ,  $\text{NO}_2$ , and  $\text{CO}$  were observed at both the urban and rural sites. The pollution levels of  $\text{SO}_2$  and  $\text{NO}_x$  were higher at the Beigongda site than at the Xin'an site while the levels of  $\text{CO}$  were similar (around 1–2 ppmv).  $\text{CO}$  has a lifetime of about 1–2 months, much longer than that of  $\text{SO}_2$  and  $\text{NO}_x$  (about one day). Compared to traffic and industrial activities, biomass burning produces relatively more  $\text{CO}$  than the other pollutants like  $\text{NO}_x$  due to inefficient combustion (Crutzen and Andreae, 1990), and it is more widespread across the rural areas, contributing nearly 20 % to the annual total  $\text{CO}$  emission in Huabei (Zhao et al., 2011). Comparing the 90th percentiles of  $\text{CO}$  at the two sites, it is expected that  $\text{CO}$  at Xin'an is more frequently affected by plume episodes from industrial and biomass burning sources. During the campaign, the Xin'an site was also influenced by air masses from the industrial areas of Tangshan, Beijing, and Tianjin (Pan et al., 2009). Biomass burning might also lead to enhanced  $\text{CO}$  at the Xin'an site. Lin et al. (2008) observed an unexpected increase of  $\text{CO}$  at Guocheng, a rural site 110 km southwest of Beijing in May, June, and October, and argued that biomass burning is a major source of  $\text{CO}$  in the agricultural areas of the region.

Diurnal cycle patterns of low-reactive primary pollutants are affected by both the source distribution and planetary boundary layer (PBL) dynamics. As shown in Fig. 6, the  $\text{NO}$ ,  $\text{NO}_2$ , and  $\text{CO}$  at Beigongda and Xin'an stations had a similar diurnal pattern with a maximum in the early morning and a minimum in the afternoon. These pollutants have strong surface sources and tend to accumulate during nighttime when the PBL is shallow while being more diluted during daytime when the PBL deepens. There was a sharp peak of  $\text{NO}$  in the early morning at the two sites, probably related to rush hour emissions, subsequent PBL deepening and  $\text{NO}_2$  photolysis. Due to the reaction of  $\text{NO}$  with  $\text{O}_3$ ,  $\text{NO}_x$  exists mainly in the form of  $\text{NO}_2$  during nighttime.

## The IPAC-NC field campaign

J. Z. Ma et al.

Title Page

Abstract

Introduction

Conclusions

References

Tables

Figures

◀

▶

◀

▶

Back

Close

Full Screen / Esc

Printer-friendly Version

Interactive Discussion





NO can be produced rapidly by the photodissociation of  $\text{NO}_2$  in the early morning at sunrise. In the afternoon, NO decreases due to the reaction with increasing  $\text{O}_3$  formed in the photochemical smog. Note that such an NO early morning peak was also observed in other rural and urban sites in China, e.g., at the Shangdianzi regional background station of Huabei (Lin et al., 2008) and at an urban station in Shanghai (Geng et al., 2008). Interestingly, the diurnal cycles of  $\text{SO}_2$  at Beigongda and Xin'an stations were similar, with higher concentrations appearing during daytime, in contrast to NO,  $\text{NO}_2$  and CO. This was also observed at the Gucheng and Shangdianzi sites in Huabei (Lin et al., 2008, 2009). Different from other primary pollutants (NO,  $\text{NO}_2$  and CO), the emissions of  $\text{SO}_2$  are dominated by coal burning in industrial activities, which contributes nearly 90% of the total  $\text{SO}_2$  emission in Huabei (Zhao et al., 2011). The plume rise by some stacks, especially of power plants, can be high enough to release the pollutants well above the stable PBL height at night. During daytime, an increase in the mixing layer brings overhead plumes to the ground, thus enhancing the  $\text{SO}_2$  concentrations as observed at these stations. A layer of enhanced  $\text{SO}_2$  at altitudes of around 500 m was observed by aircraft in IPAC-NC as presented below (see Sect. 3.3).

The diurnal cycles of secondary pollutants are mainly controlled by photochemical processes. As shown in Fig. 6, the daily  $\text{O}_3$  variation at Beigongda and Xin'an stations are typical for photochemical pollution. Hourly mean  $\text{O}_3$  concentrations at the two sites were similar, with maximum values around 65 ppbv in the afternoon. These values are more than 10 ppbv higher than the maximum hourly mean  $\text{O}_3$  concentrations observed at Xianghe, a rural site between Beigongda and Xin'an stations, in March 2005 (Li et al., 2007). In the afternoon, the  $\text{O}_3$  variability was larger at Beigongda than at Xin'an, indicating greater source dynamics and photochemistry in the urban atmosphere. The chemical cycle of NO,  $\text{NO}_2$  and  $\text{O}_3$  during sunlight is very rapid (1–2 min), and thus part of the  $\text{O}_3$  formed via the reaction of NO with  $\text{HO}_2$  and  $\text{RO}_2$  can exist in the form of  $\text{NO}_2$  when NO levels are very high. Therefore, total oxidant ( $\text{O}_x \equiv \text{O}_3 + \text{NO}_2$ ) has often been

## The IPAC-NC field campaign

J. Z. Ma et al.

[Title Page](#)[Abstract](#)[Introduction](#)[Conclusions](#)[References](#)[Tables](#)[Figures](#)[◀](#)[▶](#)[◀](#)[▶](#)[Back](#)[Close](#)[Full Screen / Esc](#)[Printer-friendly Version](#)[Interactive Discussion](#)

**The IPAC-NC field campaign**

J. Z. Ma et al.

[Title Page](#)[Abstract](#)[Introduction](#)[Conclusions](#)[References](#)[Tables](#)[Figures](#)[◀](#)[▶](#)[◀](#)[▶](#)[Back](#)[Close](#)[Full Screen / Esc](#)[Printer-friendly Version](#)[Interactive Discussion](#)

used to characterize photochemical  $O_3$  production especially in the urban and suburban areas (e.g., Lu et al., 2010). Figure 6 shows that the observed  $O_x$  concentrations at Beigongda were higher than they were at Xin'an (93 ppbv vs. 83 ppbv maximum mixing ratios), and their variability was smaller compared to  $O_3$  at Beigongda. The difference between the maximum and minimum hourly mean  $O_3$  concentration at the two sites was nearly the same (50–51 ppbv). However, the difference between the maximum and minimum hourly mean  $O_x$  concentration was smaller in Beigongda (31 ppbv) than in Xin'an (39 ppbv), both much lower than the  $O_3$  difference at the two sites. Scatter plots of measurement data show that observed  $O_3$  and  $NO_2$  were anti-correlated at the Beigongda and Xin'an stations (not shown). This indicates that  $O_3$  production at the two sites might be generally  $NO_x$ -saturated and was limited more strongly by a relatively low OH recycling efficiency with increasing  $NO_2$  at the urban site compared to the rural site. Note that the observed  $NO_2$  concentration at the Beigongda site was about 1.6 times higher than at Xin'an, and that the  $NO_2/NO$  ratio around noon was about 4.5 at Beigongda and 3.5 at Xin'an.

During the IPAC-NC campaign air samples were obtained at the Beigongda and Xin'an stations for non-methane hydrocarbon (NMHC) analyses (Cheng and Wang, 2010). Figure 7 presents the concentrations of NMHCs including alkanes, alkenes and aromatics at different local standard time (Beijing Time) as measured at the Beigongda and Xin'an stations. The average mixing ratio of NMHCs was  $118 \pm 48$  ppbv at the urban site and  $55 \pm 46$  ppbv at the rural site, and their diel variations were not significant. These NMHC levels were much higher than measured in Beijing and the surrounding area as reported by Shao et al. (2009) for the summer period. Aromatics contributed strongly to the total NMHC at both the urban (55 %) and rural (58 %) sites, followed by alkanes with a contribution of 27 % (urban) and 35 % (rural), respectively. The primary species in the aromatics included toluene, benzene and xylene. The ratio of toluene/benzene (t/b) is an important index for identifying the source contribution by automobile exhausts to the NMHCs (Zhang et al., 2008a; Geng et al., 2008; Yuan et al., 2009). Based on measurements made during IPAC-NC, the t/b ratio was 1.22 at

the Beigongda site and 0.95 at the Xin'an site. The detection probability was 100 % for both toluene and benzene at Beigongda, and at Xin'an it was 34 % for toluene and 74 % for benzene, respectively. These values indicate that the NMHCs at the urban site came mainly from automobile exhausts while they had important additional sources at the rural site.

### 3.2 Widespread air pollution in the lower atmosphere

Figure 8 shows the spatial distributions of major gaseous air pollutants measured by aircraft below 1.5 km altitude (representative of the PBL during daytime) and above 1.5 km (representative of the lower FT). Widespread high SO<sub>2</sub> mixing ratios were observed, typically of 20–40 ppbv below 1.5 km and 10–30 ppbv aloft. Over the highly polluted area near Tianjin, SO<sub>2</sub> even reached up to 60–100 ppbv in the PBL, much higher than at the surface in Xin'an (Fig. 6). These high SO<sub>2</sub> levels indicate widespread, strong and elevated industrial emission sources across the region. The SO<sub>2</sub> levels observed in this study are a few times higher than those measured over Northeastern China in April 2005 and an order of magnitude higher than those over the Northeastern United States (Dickerson et al., 2007). Contrary to SO<sub>2</sub>, CO in the PBL was lower aloft than at the surface, indicating other CO sources rather than the elevated industrial stacks. Nevertheless, high CO mixing ratios around 1 ppmv were also observed within the pollution pool during some flights. Note that the CO data are not as complete as for the other trace gases due to an instrument problem as described above (Sect. 2.3).

NO was typically a few ppbv during all flights below and above 1.5 km altitude. As shown in Fig. 8, relatively low NO (<1 ppbv) was observed along the circular flight path of RF01 over a rural area in Tianjin (near the Xin'an station) on 9 April 2006 (see Table 2 and Fig. 4 for flight information). Higher NO mixing ratios (1–2 ppbv) were observed during another circular flight, RF06, over the Bohai Gulf on 17 April 2006. Heavy cloudy conditions were encountered on 9 April 2006, with both cloud fraction and the liquid water content being highest during the campaign (Ma et al., 2010). A severe dust storm episode was observed on 17 April 2006 (Wang et al., 2008). The combined

## The IPAC-NC field campaign

J. Z. Ma et al.

Title Page

Abstract

Introduction

Conclusions

References

Tables

Figures

◀

▶

◀

▶

Back

Close

Full Screen / Esc

Printer-friendly Version

Interactive Discussion



cloud and dust conditions resulted in a remarkably strong decrease in the photolysis rate of  $\text{NO}_2$  and thus a lower  $\text{NO}/\text{NO}_2$  ratio in the PBL.

Although the aircraft  $\text{NO}_x^*$  measurements are likely to include some nitric acid and organic nitrates, it may be used as an indicator of the  $\text{NO}_x$  pollution level over the region investigated during IPAC-NC. The  $\text{NO}_x^*$  levels during the campaign were generally 10–20 ppbv below 1.5 km altitude and 2–10 ppbv aloft. Similar to  $\text{SO}_2$  and CO, highest  $\text{NO}_x^*$  concentrations were observed in the highly polluted area, with maximum mixing ratios up to 30–50 ppbv. These high  $\text{NO}_x^*$  levels corroborate the existence of the pollution pool in the lower atmosphere. With respect to pollution levels over the Bohai Gulf, the  $\text{SO}_2$  and  $\text{NO}_x$  concentrations observed in this study are comparable to those observed in March 2002 by Hatakeyama et al. (2005). The emission rates of these pollutants in the Huabei region may nevertheless have increased strongly from 2002 to 2006 (Zhang et al., 2009b). Since the number of flights was rather small over the Bohai Gulf in both campaigns, the measurement data set does not suffice to derive emission trends. Although the observed  $\text{O}_3$  is expected to have been primarily produced from the photochemical oxidation of CO and VOCs catalyzed by  $\text{NO}_x$ , during spring stratospheric intrusions may contribute to tropospheric ozone (Hocking et al., 2007). The mixing ratios of  $\text{O}_3$  were typically 30–50 ppbv during the campaign. The highest  $\text{O}_3$  mixing ratios of 60–70 ppbv were observed in the severely polluted area.

### 3.3 Vertical profiles

Figure 9 presents the vertical profiles of trace gases measured during IPAC-NC. Although strongly enhanced concentrations were found in a few plumes, the pollutants were typically more homogeneously distributed with increasing altitude. A decreasing tendency of NO,  $\text{NO}_x^*$  and CO with increasing altitude is evident. The vertical profile of  $\text{SO}_2$  shows a maximum at  $\sim 0.5$  km altitude, owing to the predominantly elevated emissions from large industrial sources. Together with the diurnal variation of the PBL a distinct temporal pattern of  $\text{SO}_2$  is apparent near the surface, as described above (Sect. 3.1) and in previous studies (Lin et al., 2008, 2009). Due to weaker titration and

## The IPAC-NC field campaign

J. Z. Ma et al.

Title Page

Abstract

Introduction

Conclusions

References

Tables

Figures

◀

▶

◀

▶

Back

Close

Full Screen / Esc

Printer-friendly Version

Interactive Discussion



**The IPAC-NC field campaign**

J. Z. Ma et al.

Title Page

Abstract

Introduction

Conclusions

References

Tables

Figures

◀

▶

◀

▶

Back

Close

Full Screen / Esc

Printer-friendly Version

Interactive Discussion



the active photochemistry, relatively high  $O_3$  concentrations may occur near the top of the mixing layer ( $\sim 100$  m above the surface). However, such  $O_3$  peaks could not be observed during IPAC-NC since our aircraft was not allowed to fly below 400 m above the ground. The  $O_3$  mixing ratios were generally higher near the surface compared to higher altitudes within the PBL. These vertical profiles are similar to the tropospheric ozone climatology over Beijing as observed in the MOZAIC program (Ding et al., 2008). A remarkable  $O_3$  increase at an altitude of 0.5–1.5 km was observed over Beijing during the summer afternoon (Ding et al., (2008). An elevated pollution layer was also observed over Beijing at 2500–3500 m altitude during summer, attributed to a mountain chimney effect (Chen et al., 2009). The increases in  $O_3$  and other pollutants at these altitudes were generally not significant over the Tianjin, Tangshan and Bohai area during the spring IPAC-NC campaign although some episodic enhancements were observed. Note that our aircraft may have missed such profiles since the chemistry instruments were switched off during take-off and landing at Tianjin airport. A summary of daytime meteorological parameters and trace gas concentrations, including NMHCs, observed during IPAC-NC is given in Table 3. The data obtained at the Xin'an site are assumed to be representative for the region at the surface.

### 3.4 Estimated radical concentrations

We calculated radical concentrations and chemical reaction rates with a chemical box model based on the NCAR Master Mechanism (Madronich and Calvert, 1989, 1990; Ma et al., 2002b), constrained by the observed mean trace gas concentrations shown in Fig. 9 as well as in Table 3. Eight altitude levels, 0.0 km, 0.4 km, 0.8 km, 1.2 km, 1.6 km, 2.0 km, 2.4 km and 2.8 km, were selected for the calculations. During each simulation, specified physical and chemical parameters such as temperature and the mixing ratios of relatively long-lived species such as  $H_2O$ ,  $CH_4$ ,  $H_2$ ,  $SO_2$ ,  $NO$ ,  $NO_2$ ,  $CO$ ,  $O_3$  and NMHCs, were kept constant. The concentrations of  $NO_2$  were derived by scaling measured  $NO$  with the  $NO_2/NO$  ratios derived from our RCTM (Ma et al., 2002a). The observed individual NMHC species in the field experiment were applied

## The IPAC-NC field campaign

J. Z. Ma et al.

Title Page

Abstract

Introduction

Conclusions

References

Tables

Figures

◀

▶

◀

▶

Back

Close

Full Screen / Esc

Printer-friendly Version

Interactive Discussion



as described by Ma et al. (2002b). The concentrations of  $\text{CH}_2\text{O}$ ,  $\text{CH}_3\text{OOH}$  and  $\text{H}_2\text{O}_2$  were not measured during our field experiment, and their values were taken from measurements taken in other studies. For example, the initial  $\text{CH}_2\text{O}$  concentration was assumed 5 ppbv at the surface, increasing to 1.5 ppbv at 1.6 km altitude (Russo et al., 2003; Shao et al., 2009). Photodissociation rate coefficients (J-values) were calculated with the radiation transfer model TUV (Madronich, 1987), and the daytime mean J-values for 15 April 2006 were used for model simulations at the selected altitudes. Clear sky conditions were adopted, and the mean vertical profiles of aerosol optical properties, based on our aircraft measurements (Ma et al., 2010), were used in the J-value calculations.

We took into account heterogeneous reactions of trace gases and radicals on aerosol surfaces in the model simulations:



Figure 10 shows the mean distributions of aerosol number concentrations and particle surface areas as a function of altitude, used in the calculations of photolysis rates and heterogeneous reactions (Ma et al., 2010). It was demonstrated that the number concentrations of aerosol particles were dominated by the nucleation mode and lower Aiken mode ( $5\text{nm} < D_p < 100\text{nm}$ ) at higher altitudes ( $> \sim 1.5\text{ km}$ ) and by the Aiken mode and lower accumulation mode ( $20\text{nm} < D_p < 200\text{nm}$ ) at lower altitudes ( $< \sim 1.5\text{ km}$ ). Correspondingly, the aerosol surface areas were dominated by the accumulation mode with a peak centered at  $D_p \approx 200\text{ nm}$  and to a lesser extent by the coarse mode with a peak centered at  $D_p \approx 1.5\text{ }\mu\text{m}$ , the latter being related to dust aerosols. The total number density of aerosols was about  $1.4 \times 10^4\text{ particles cm}^{-3}$  near the surface, and  $1.7 \times 10^4$  and  $3.0 \times 10^4\text{ particles cm}^{-3}$  at 1 and 2 km altitudes, respectively. The surface area concentration of aerosols was about  $3.8 \times 10^2\text{ }\mu\text{m}^2\text{ cm}^{-3}$  near the surface, and  $2.4 \times 10^2$  and  $1.3 \times 10^2\text{ }\mu\text{m}^2\text{ cm}^{-3}$  at 1 and 2 km altitude, respectively.

We adopted the same values of uptake coefficients as used by Zhu et al. (2010) for the calculation of heterogeneous reaction rates.

$$k_{\gamma} = \int \left[ \frac{1 + Kn}{1 + 0.377 Kn + 1.33 Kn \cdot (1 + Kn) / \gamma} \right] \cdot 4\pi \cdot D_v \cdot r \cdot N \cdot dr \quad (1)$$

where  $k_{\gamma}$  is the pseudo first-order rate coefficient ( $\text{s}^{-1}$ ),  $Kn$  is the Knudsen number (the ratio of mean free path of condensing vapor molecules to particle radius),  $\gamma$  is the uptake coefficient of a species,  $D_v$  is the diffusion coefficient of the condensing vapor ( $\text{cm}^2 \text{s}^{-1}$ ),  $r$  and  $N$  represent the particle radius (cm) and number concentration ( $\text{cm}^{-3}$ ) with a radius between  $r$  and  $r + dr$ . All organic carbonyls, alcohols and peroxides, and acids in the model are assumed to have the same reactive uptake coefficients as  $\text{CH}_2\text{O}$ ,  $\text{CH}_3\text{OOH}$  and  $\text{CH}_3\text{COOH}$ , respectively. The chemical rate equations were integrated forward with a Gear-type solver. Simulations were performed for 12 h and the results of the last hour are analyzed in this study. Since most long-lived species were fixed, the concentrations of radicals and other organic products could attain a steady state during the last few hours with changes less than 1%. We considered three scenarios in the model simulations. BASE refers to the standard simulation, and NO\_S and NO\_H are sensitivity simulations without considering  $\text{SO}_2$  associated reactions and heterogeneous reactions of OH and  $\text{HO}_2$  on aerosol surfaces, respectively.

Figure 11a and b presents the calculated vertical profiles of OH and  $\text{HO}_2$  concentrations, respectively. Interestingly, we find a peak in the vertical profiles of both OH and  $\text{HO}_2$  at about 1 km altitude. From the base run, the OH concentration is calculated to be  $5.4 \times 10^6$  molecules  $\text{cm}^{-3}$  ( $\sim 0.22$  pptv) at the surface, increasing to  $6.9 \times 10^6$  molecules  $\text{cm}^{-3}$  ( $\sim 0.29$  pptv) at 0.8 km altitude, and dropping to  $4.7 \times 10^6$  molecules  $\text{cm}^{-3}$  ( $\sim 0.22$  pptv) and  $3.8 \times 10^6$  molecules  $\text{cm}^{-3}$  ( $\sim 0.19$  pptv) at 1.6 km and 2.4 km, respectively. The profile of  $\text{HO}_2$  is similar to that of OH, with a maximum of  $1.8 \times 10^8$  molecules  $\text{cm}^{-3}$  ( $\sim 7.6$  pptv) at 0.8 km. The surface level of OH in the polluted rural area of Huabei estimated in this study is comparable to that in the Mexico City Metropolitan Area (MCMA) and higher than that in New York City

**The IPAC-NC field campaign**

J. Z. Ma et al.

Title Page

Abstract

Introduction

Conclusions

References

Tables

Figures

◀

▶

◀

▶

Back

Close

Full Screen / Esc

Printer-friendly Version

Interactive Discussion



**The IPAC-NC field campaign**

J. Z. Ma et al.

Title Page

Abstract

Introduction

Conclusions

References

Tables

Figures

◀

▶

◀

▶

Back

Close

Full Screen / Esc

Printer-friendly Version

Interactive Discussion



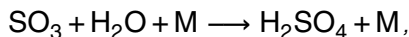
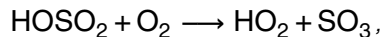
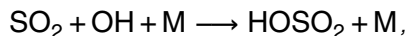
(NYC). According to the measurements by Ren et al. (2003) and Shirley et al. (2006), the diurnal peak of median OH was 0.28 pptv at NYC in July 2001 and 0.35 pptv ( $\sim 7 \times 10^6$  molecules  $\text{cm}^{-3}$ ) at MCMA in April 2003. A high average OH concentration of  $15 \times 10^6$  molecules  $\text{cm}^{-3}$  around noon was observed in the polluted rural area of the Pearl River Delta (PRD) in China during July 2006, and this could not be reproduced by the model calculations of Hofzumahaus et al. (2009). Our OH estimate for Huabei is much lower than observed in the PRD, but it is comparable to the OH simulated for PRD (the latter with a diurnal peak of  $\sim 7 \times 10^6$  molecules  $\text{cm}^{-3}$ ). Unaccounted OH recycling remains to be a challenge, and it is conceivable that our model also underestimates OH (Lelieveld et al., 2008; Hofzumahaus et al., 2009).

Measurements of OH vertical profiles are sparse compared to ground-based observations. As reviewed by Singh et al. (2009), INTEX-B provided detailed vertical distributions of OH measured over the Gulf of Mexico and the subtropical Pacific in spring 2006, during the same season as the IPAC-NC campaign. OH levels in the lower atmosphere estimated for Huabei are similar to those over the Gulf of Mexico and 2–3 times higher than those over the subtropical Pacific. The mean vertical profile of OH, derived for Huabei, is also similar to that over the Gulf of Mexico, the latter having a peak around  $\sim 0.3$  pptv at an altitude of 3–4 km a.s.l., as shown by Singh et al. (2009) (note that MCMA is at an altitude of 2240 m a.s.l.). A similar OH profile was observed over the Suriname rainforest during the GABRIEL campaign, with a peak concentration at 2–3 km altitude (Lelieveld et al., 2008; Kubistin et al., 2010). The transport and evolution of Asian pollution over the Pacific have been thought to have a substantial impact on surface air quality along the west coast of North America (Zhang et al., 2008b; Singh et al., 2009). Higher OH concentrations in the lower atmosphere over Huabei, one of the most severely polluted regions in Asia, compared to those over the Pacific indicate that primary pollutants are efficiently oxidized before being transported across the Pacific to North America. Huabei is not only a highly polluted region but also acts as an oxidation pool over China.

### 3.5 HO<sub>x</sub> radical budget and relevant chemical reactions

An overview of the most relevant reactions for the HO<sub>x</sub> budget over the polluted region of Huabei is given in Tables 4 and 5. The photolysis of ozone followed by reaction with water vapor, together called the effective photolysis of ozone (Ma and Weele, 2000; Ma et al., 2002b), is the main source of tropospheric OH on a global scale (Rohrer and Berresheim, 2006; Lelieveld et al., 2002b). In contrast, in the lower atmosphere over Huabei this primary OH production merely contributes 6–7 % to the total production of OH. The OH radical recycling by reaction NO + HO<sub>2</sub> makes a dominant contribution (90 ± 3%) to the total production. At the surface, the contribution of HNO<sub>2</sub> photolysis (2.4 %) is comparable to that of ozone photolysis (1.6 %), in accord with previous results for polluted areas (Volkamer et al., 2010 and references therein). In addition to gas-phase chemistry, heterogeneous reactions on aerosol surfaces and the release from soil nitrate have been suggested as important sources of HNO<sub>2</sub> (Ammann et al., 1998; Stemmler et al., 2006; Su et al., 2008, 2011; An et al., 2009), though not included in our model. The contributions of other reactions, including the photolysis of H<sub>2</sub>O<sub>2</sub>, are much less (~1 %).

Our model analysis suggests that the loss of OH over the polluted region of Huabei is dominated by the reaction with CO (15–33 %), followed by the reaction with NO<sub>2</sub> (14–21 %). Interestingly, we find that the reaction with SO<sub>2</sub> also makes a substantial contribution (15–16%) to the OH loss in the lower atmosphere, i.e. well above the ground, owing to high levels of SO<sub>2</sub> over the region.



## The IPAC-NC field campaign

J. Z. Ma et al.

Title Page

Abstract

Introduction

Conclusions

References

Tables

Figures

I◀

▶I

◀

▶

Back

Close

Full Screen / Esc

Printer-friendly Version

Interactive Discussion



Due to its short lifetime ( $\tau_{\text{OH}} < 0.1$  s), OH rapidly reaches a steady state between production and loss.

$$\frac{d[\text{OH}]}{dt} = P(\text{OH}) - k_{\text{OH}} \cdot [\text{OH}] \approx 0. \quad (2)$$

The pseudo first-order rate coefficient of OH ( $k_{\text{OH}}$ ), i.e., the inverse of the atmospheric OH lifetime ( $\tau_{\text{OH}}^{-1}$ ), is an important parameter that has been used to measure the total OH reactivity in the atmosphere (e.g., Mao et al., 2009; Sheehy et al., 2010; Sinha et al., 2010; Lou et al., 2010).

$$k_{\text{OH}} = \sum_i k_{\text{OH}+\text{X}_i} \cdot [\text{X}_i] = \tau_{\text{OH}}^{-1}, \quad (3)$$

where  $[\text{X}_i]$  is the concentration of a reactive species (CO, NO<sub>2</sub>, SO<sub>2</sub>, VOCs etc.) in ambient air,  $k_{\text{OH}+\text{X}_i}$  represents the corresponding bimolecular reaction rate constant, and  $k_{\text{OH}+\text{X}_i} \cdot [\text{X}_i]$  stands for the reactivity of X<sub>i</sub>.  $k_{\text{OH}}$  values were observed between 1 s<sup>-1</sup> in clean air and 200 s<sup>-1</sup> in heavily polluted air in the atmospheric boundary layer (Lou et al., 2010, and references therein). The daytime average OH reactivity during IPAC-NC is estimated to be 44 s<sup>-1</sup> on the ground, and 12, 8 and 6 s<sup>-1</sup> at altitudes of 0.8, 1.6 and 2.4 km, respectively. The OH reactivity over Huabei estimated in this study is much higher than that in the lower atmosphere over the Pacific, where a median  $k_{\text{OH}}$  value of  $4.0 \pm 1.0$  s<sup>-1</sup> was measured by aircraft during INTEX-B (Mao et al., 2009). Note that the total OH reactivity generally varies during the day (Sheehy et al., 2010; Lou et al., 2010). For example, surface  $k_{\text{OH}}$  in the PRD was observed to have a mean maximum value of 50 s<sup>-1</sup> at daybreak and a mean minimum value of 20 s<sup>-1</sup> at noon (Lou et al., 2010). About 35–45 % of the total OH reactivity in IPAC-NC appears to come from reactions with VOCs. In contrast, previous studies indicated that the OH reactivity in polluted areas was dominated by organic compounds, e.g., 70 % in MCMA (Shirley et al., 2006) and 85 % in the PRD (Lou et al., 2010).

The main source of HO<sub>2</sub> over the polluted region of Huabei is the reaction of OH with CO (17–34 %). In the upper part of the PBL and the lower FT, the contribution from

## The IPAC-NC field campaign

J. Z. Ma et al.

Title Page

Abstract

Introduction

Conclusions

References

Tables

Figures

◀

▶

◀

▶

Back

Close

Full Screen / Esc

Printer-friendly Version

Interactive Discussion



photolysis of  $\text{CH}_2\text{O}$  (9–15%) is also considerable. Again, we find that the reaction of OH with  $\text{SO}_2$  makes a substantial contribution (16–18%) to the  $\text{HO}_2$  production in the upper part of the PBL and the lower FT. To our knowledge, such efficient recycling between OH and  $\text{HO}_2$  by  $\text{SO}_2$ -involved reactions was not found in previous studies.

Kanaya et al. (2009) reported a much smaller (3%) contribution of reaction  $\text{SO}_2 + \text{OH}$  to the  $\text{HO}_2$  production over East China during the Mount Tai Experiment 2006. During IPAC-NC, the oxidation of VOCs contributes ~75% to the  $\text{HO}_2$  production near the surface and 50–65% in the upper part of the PBL and the lower FT. The loss of  $\text{HO}_2$  over Huabei is mainly controlled by the reaction of  $\text{HO}_2$  with NO (>94%), which recycles OH very efficiently as described above.

Note that we take into account heterogeneous reactions of radicals including OH and  $\text{HO}_2$  on aerosol surfaces in our model simulations. The calculated pseudo first-order rate coefficients for the removal of  $\text{HO}_2$  by aerosol particles are  $0.025 \text{ s}^{-1}$  at the surface and 0.018, 0.010 and  $0.006 \text{ s}^{-1}$  at altitudes of 0.8, 1.6 and 2.4 km, respectively. Correspondingly, the concentrations of  $\text{HO}_2$  decrease by 8% at the surface and by 22%, 9% and 6% when heterogeneous reactions of radicals are included (BASE) compared to the model runs in which they were not included (NO\_H), and the relative decreases of OH concentrations are similar. Kanaya et al. (2009) reported a larger effect of heterogeneous reactions on  $\text{HO}_x$  radicals over East China during the Mount Tai Experiment in June 2006, with the daytime maximum concentrations decreasing by 26% (from  $5.0 \times 10^6$  to  $3.7 \times 10^6$  molecules  $\text{cm}^{-3}$ ) for OH and 41% (from 34 to 20 pptv) for  $\text{HO}_2$ , respectively. They adopted a central value of the uptake coefficient of  $0.25 \pm 0.09$  ( $n = 10$ ), measured in their laboratory, and estimated particle size distributions with observed mass concentrations of chemical species in 9 size bins between 0.43– $9 \mu\text{m}$ . Kanaya et al. (2009) estimated a typical surface area concentration of  $6.3 \times 10^2 \mu\text{m}^2 \text{ cm}^{-3}$ , much higher than our measurements during IPAC-NC, and a median pseudo first-order rate coefficient of  $0.014 \text{ s}^{-1}$  for the removal of  $\text{HO}_2$ , comparable to our estimate at about 1 km altitude.

**The IPAC-NC field campaign**

J. Z. Ma et al.

Title Page

Abstract

Introduction

Conclusions

References

Tables

Figures

◀

▶

◀

▶

Back

Close

Full Screen / Esc

Printer-friendly Version

Interactive Discussion



**The IPAC-NC field campaign**

J. Z. Ma et al.

[Title Page](#)[Abstract](#)[Introduction](#)[Conclusions](#)[References](#)[Tables](#)[Figures](#)[◀](#)[▶](#)[◀](#)[▶](#)[Back](#)[Close](#)[Full Screen / Esc](#)[Printer-friendly Version](#)[Interactive Discussion](#)

Regardless of the uptake coefficients and aerosol particle size distributions employed, the loss efficiency of  $\text{HO}_2$  is ultimately determined by the calculated pseudo first-order rate coefficient. With similar values of the pseudo first-order rate coefficients (e.g., about  $0.015 \text{ s}^{-1}$  at 1 km altitude over Huabei), the smaller effect of heterogeneous reactions on  $\text{HO}_2$  concentration estimated in this study ( $\sim 20\%$ ) than by Kanaya et al. (2009) may be related to the difference in the treatment of intermediate VOC oxidation products between the two models. The chemical box model used by Kanaya et al. (2009) was based on the Regional Atmospheric Chemistry Mechanism (RACM) (Stockwell et al., 1997). RACM is a condensed mechanism, with a much smaller number of the intermediate VOC oxidation products (e.g., HCHO and lumped species ALD, KET and MACR) than the NCAR Master Mechanism. The more complex intermediate VOC oxidation products were prescribed in their model simulations and kept constant from the reference to the sensitivity simulations (Kanaya et al., 2009). In our model simulations, all (a few hundred) intermediate VOC oxidation products, except for HCHO and  $\text{CH}_3\text{OH}$ , were simulated to attain steady state between production and loss, the latter also including heterogeneous reactions of these compounds. Compared to the standard simulations (BASE), the sensitivity simulations without heterogeneous reactions of OH and  $\text{HO}_2$  ( $\text{NO}_x$ ) attained a new steady state with different concentrations of the intermediate VOC oxidation products. For example, the mixing ratio of  $\text{CH}_3\text{COCHO}$  at 0.8 km altitude was 0.45 ppbv in BASE and 0.54 ppbv in  $\text{NO}_x$ , respectively. Such differences in the intermediate VOC oxidation products can reduce the changes in simulated OH and  $\text{HO}_2$  relative to the simulations with fixed concentrations.

De Reus et al. (2005) investigated the effect of heterogeneous removal of  $\text{HO}_2$  on Saharan dust particles on the  $\text{RO}_x$  ( $\text{HO}_2 + \text{RO}_2$ ) mixing ratio applying an uptake coefficient of 0.2, the same as used in this study. They focused on relatively long-lived trace gases with the initial conditions from measurements and showed that heterogeneous removal of  $\text{HO}_2$  causes only a small decrease in  $\text{RO}_x$ , with the calc/obs ratio of  $\text{RO}_x$  decreasing from 1.38 in the run without heterogeneous removal reactions to 1.30 in the run with heterogeneous removal of  $\text{HO}_2$  (de Reus et al., 2005). In addition to

the direct heterogeneous loss rate, the changes in OH and HO<sub>2</sub> reflect other chemical characteristics. As presented above, we estimated a smaller decrease in OH and HO<sub>2</sub> at the surface (8 %) compared to 0.8 km altitude (22 %), with a higher first-order rate coefficient for the removal of HO<sub>2</sub> at the surface (0.025 s<sup>-1</sup>) than at 0.8 km (0.018 s<sup>-1</sup>).

5 This suggests that the atmosphere over Huabei had a stronger capacity to buffer the perturbations on HO<sub>x</sub> near the surface than in the upper part of the PBL, most probably due to higher VOC concentrations.

The reasons for the relatively high HO<sub>x</sub> radical levels in the lower atmosphere over Huabei are intricate. It appears that the effective photolysis of ozone combined with the reactions of OH with NO<sub>2</sub>, CO and SO<sub>2</sub> play an important role. First, the effective photolysis of ozone (determined by the reaction H<sub>2</sub>O + O(<sup>1</sup>D)), which acts as a primary source of HO<sub>x</sub>, has a maximum at 0.8 km altitude. The reaction rates of H<sub>2</sub>O + O(<sup>1</sup>D) are calculated to be 3.7 × 10<sup>6</sup> molecules cm<sup>-3</sup> s<sup>-1</sup> at the surface, and 4.6 × 10<sup>6</sup>, 2.7 × 10<sup>6</sup> and 1.5 × 10<sup>6</sup> molecules cm<sup>-3</sup> s<sup>-1</sup> at altitudes of 0.8, 1.6 and 2.4 km, respectively. Second, with respect to the fractional contribution to the OH loss rate, the reaction CO + OH (which recycles HO<sub>2</sub>) has a maximum (33 %) and the reaction NO<sub>2</sub> + OH (which acts as a primary sink of HO<sub>x</sub>) has a minimum (14 %) at 0.8 km. Third, the relative importance of other species, such as CH<sub>2</sub>O and SO<sub>2</sub>, also changes with altitude. The reaction rate of SO<sub>2</sub> + OH is calculated to be 6.7 × 10<sup>6</sup> molecules cm<sup>-3</sup> s<sup>-1</sup> at the surface, and 1.3 × 10<sup>7</sup>, 5.8 × 10<sup>6</sup> and 3.4 × 10<sup>6</sup> molecules cm<sup>-3</sup> s<sup>-1</sup> at altitudes of 0.8, 1.6 and 2.4 km, respectively, with a maximum at 0.8 km. CO and SO<sub>2</sub> also compete with NO<sub>2</sub> to react with OH, recycling HO<sub>2</sub> without a loss of total HO<sub>x</sub>. VOC oxidation can play an important role in recycling OH, sustaining the atmospheric oxidation capacity and amplifying trace gas removal in the troposphere (Lelieveld et al., 2008; Hofzumahaus et al., 2009). The effects of VOC oxidation on the HO<sub>x</sub> budget deserve scrutiny and will be detailed in future work, for example to study the role of aromatics in HO<sub>x</sub> recycling.

**The IPAC-NC field campaign**

J. Z. Ma et al.

Title Page

Abstract

Introduction

Conclusions

References

Tables

Figures

◀

▶

◀

▶

Back

Close

Full Screen / Esc

Printer-friendly Version

Interactive Discussion



### 3.6 Ozone and secondary aerosol formation

Figure 11c presents the vertical profile of net ozone production over the polluted region of Huabei calculated with the NCAR Master Mechanism. Table 6 presents an overview of the most relevant reactions for the ozone budget. As previous studies (e.g., Liu et al., 1987; Ma et al., 2002b; Lu et al., 2010), the total oxidant ( $O_x \equiv O_3 + NO_2$ ) is used to infer instantaneous photochemical production,  $P(O_3)$ , and loss,  $L(O_3)$ , of ozone.

$$P(O_3) = k_7 \cdot [HO_2] \cdot [NO] + \sum k_6 \cdot [RO_2] \cdot [NO]. \quad (4)$$

$$L(O_3) = k_1 \cdot [O(^1D)] \cdot [H_2O] + k_9 \cdot [HO_2] \cdot [O_3] + k_{10} \cdot [OH] \cdot [O_3] + \sum k_{11} \cdot [\text{alkene}] \cdot [O_3] + k_{12} \cdot [NO_2] \cdot [OH]. \quad (5)$$

$P(O_3)$  in the lower atmosphere over Huabei is calculated to be  $48 \text{ ppbv h}^{-1}$  at the surface, and 16, 8 and  $5 \text{ ppbv h}^{-1}$  at altitudes of 0.8, 1.6 and 2.4 km, respectively. The recycling of OH through the reaction of  $HO_2$  with NO and the associated photolysis of  $NO_2$  is the main process (65–74 %) leading to ozone formation, followed by the reaction of  $CH_3O_2$  with NO (~6 %).  $L(O_3)$  is calculated to be  $9 \text{ ppbv h}^{-1}$  at the surface, and 3, 2 and  $1 \text{ ppbv h}^{-1}$  at altitudes of 0.8, 1.6 and 2.4 km, respectively. The reaction of  $NO_2$  with OH is the dominant ozone loss process (62–70 %). At the surface ~16 % of  $O_3$  loss is attributed to its reaction with 2-butene. At higher altitudes, the effective photolysis of  $O_3$  becomes more important, contributing 11–13 % to  $L(O_3)$ . It is estimated that 8–15 % of the  $O_3$  loss is due to its reaction on aerosol surfaces.

The calculated near-surface rate of  $P(O_3)$  during IPAC-NC is comparable to the maximum  $P(O_3)$  ( $50 \text{ ppbv h}^{-1}$ ) at a suburban location near Beijing reported by Lu et al. (2010). Our  $P(O_3)$  and  $P(O_3)-L(O_3)$  rates at higher altitudes (e.g., 9.3–5.3 and 7.4–4.0  $\text{ppbv h}^{-1}$  at 1.6–2.4 km in the case of NO<sub>2</sub>-HR) are comparable to the daytime 6-h average  $P(O_3)$  and  $P(O_3)-L(O_3)$  values (7.9 and 6.4  $\text{ppbv h}^{-1}$ ) over East China during the Mount Tai Experiment 2006 (Kanaya et al., 2009). Kanaya et al. (2009) showed that the heterogeneous loss of  $HO_2$  on aerosols reduced the daytime 6-h average net

ozone production rate,  $P(\text{O}_3)\text{-L}(\text{O}_3)$ , by  $2.1 \text{ ppbv h}^{-1}$  (from  $6.4 \text{ ppbv h}^{-1}$ ). Our model sensitivity runs show a smaller effect with  $P(\text{O}_3)\text{-L}(\text{O}_3)$  decreasing to  $6.7 \text{ ppbv h}^{-1}$  from  $7.4 \text{ ppbv h}^{-1}$  (by  $0.7 \text{ ppbv h}^{-1}$ ) at 1.6 km altitude. Our results suggest that the net ozone production in the lower atmosphere over Huabei during IPAC-NC (e.g.,  $16 \text{ ppbv h}^{-1}$  at 0.8 km) is much higher than the average of  $>5 \text{ ppbv d}^{-1}$  (at 800 hPa) over the polluted part of the Asian continent during INTEX-B as simulated with a global model by Zhang et al. (2008b).

At high  $\text{NO}_x$  levels, e.g., over the polluted Huabei region, the photochemical ozone buildup is limited by radical formation and thus by the oxidation of CO and VOCs. As discussed above,  $P(\text{O}_3)$  in the lower atmosphere over Huabei is dominated by the reaction of  $\text{HO}_2$  with NO (by 65–74 %), and the production of  $\text{HO}_2$  is dominated by the reaction of CO with OH (17–34 %). Therefore, we estimate that the oxidation of CO makes contributions to  $P(\text{O}_3)$  of 14 % ( $\sim 6.7 \text{ ppbv h}^{-1}$ ) at the surface, and 25 % ( $\sim 3.8 \text{ ppbv h}^{-1}$ ), 13 % ( $\sim 1.1 \text{ ppbv h}^{-1}$ ) and 12 % ( $\sim 0.6 \text{ ppbv h}^{-1}$ ) at altitudes of 0.8, 1.6 and 2.4 km, respectively. The contribution of the reaction  $\text{NO} + \text{HO}_2$  to  $P(\text{O}_3)$  is greatest (74 %) at 0.8 km, where the reaction  $\text{SO}_2 + \text{OH}$  adds 17 % to the  $\text{HO}_2$  production. This indicates that the oxidation of  $\text{SO}_2$  remarkably augments ozone formation (up to  $\sim 13\%$  or  $2.0 \text{ ppbv h}^{-1}$  at 0.8 km) in the lower atmosphere over Huabei. The oxidation of VOCs contributes most strongly to  $P(\text{O}_3)$  near the surface,  $\sim 85\%$ , of which  $\sim 50\%$  through the reaction  $\text{HO}_2 + \text{NO}$  and  $\sim 35\%$  through  $\text{RO}_2 + \text{NO}$ . At higher altitudes the contribution of VOCs to  $P(\text{O}_3)$  is 60–75 %, of which about 35–45 % through  $\text{HO}_2 + \text{NO}$  and 25–30 % through  $\text{RO}_2 + \text{NO}$ .

In the highly active oxidative atmospheric environment over Huabei primary gaseous pollutants such as  $\text{SO}_2$ ,  $\text{NO}_2$  and VOCs are efficiently converted into less volatile species such as sulfuric, nitric and organic acids that can partition into the condensed phase. It has been shown previously that high OH levels can substantially affect condensation rates onto aerosol particles (Robinson et al., 2007; Ma et al., 2010). We used the chemical box model, constrained by the measurements, to compute the formation of condensable intermediate and terminal oxidation products such as organic

**The IPAC-NC field campaign**

J. Z. Ma et al.

Title Page

Abstract

Introduction

Conclusions

References

Tables

Figures

◀

▶

◀

▶

Back

Close

Full Screen / Esc

Printer-friendly Version

Interactive Discussion



acids from the oxidation of VOCs. The concentrations of these species were calculated by assuming steady state between their chemical production and loss. Since we do not account for gas-particle partitioning as a function of aerosol composition and ambient conditions (Farina et al., 2010), these production rates represent upper limits of the rates of condensation (called condensation potential).

Figure 12 presents the vertical distributions of sulfuric acid and VOC oxidation products and their condensation potentials onto aerosol surfaces over the polluted region of Huabei during IPAC-NC. The several hundred VOC oxidation products have been subdivided into functional groups including organic peroxides, organic nitrates, organic carbonyls, organic acids, and the total of organic reaction products (the sum of these individual groups). The condensation potential of sulfuric acid is estimated to be  $2\text{--}8\ \mu\text{g cm}^{-3}\ \text{h}^{-1}$ , with a peak value at an altitude of 0.8 km. Considering the low volatility of sulfuric acid, this potential approximates the actual condensation rate. During IPAC-NC, the average mass concentrations of sulfate and organic aerosols (OA) in  $\text{PM}_{10}$  measured by aircraft were 9 and  $10\ \mu\text{g cm}^{-3}$ , respectively (Ma et al., 2010). This indicates that it takes a few hours for the gas-phase chemical transformation mechanisms to produce the amount of sulfate in aerosols sampled during IPAC-NC.

The relative contribution of primary organic aerosols (POA) and secondary organic aerosols (SOA) to the overall OA budget is to some degree controversial, and recent studies have highlighted the importance of intermediate-volatile SOA (typically with  $12 < C < 21$ ) (Robinson et al., 2007; de Gouw et al., 2011). As shown in Fig. 12, the condensation potential of total organics is much lower than that of sulfuric acid, with a maximum value of  $\sim 0.5\ \mu\text{g cm}^{-3}\ \text{h}^{-1}$  at the surface. Based on these formation rates, we estimate that during IPAC-NC the SOA formed from the gas phase chemical transformation of VOCs on preexisting particles (e.g., dust) was 1 and  $5\ \mu\text{g cm}^{-3}$  during periods of 1 and 10 h, respectively. Recall that the calculated condensation potential provides an upper bound. Due to limitations in both the VOC sample analyses and the model chemical mechanism, we did not consider the oxidation of organic compounds with  $C > 9$ , which tend to have a relatively low volatility (de Gouw et al., 2011). In

**The IPAC-NC field campaign**

J. Z. Ma et al.

Title Page

Abstract

Introduction

Conclusions

References

Tables

Figures

◀

▶

◀

▶

Back

Close

Full Screen / Esc

Printer-friendly Version

Interactive Discussion



view of the measured  $\sim 10 \mu\text{g cm}^{-3}$  of OA in  $\text{PM}_{10}$ , it seems that substantial additional oxidation of VOCs than accounted for here, including reactions with  $\text{C} > 9$ , contributed to SOA formation during IPAC-NC. Furthermore, directly emitted OA, e.g. from biomass burning, may have contributed substantially as well.

## 4 Summary and conclusions

Recently, regional air pollution, characterized by photochemical smog and grey haze-fog, has become a severe environmental problem in China. We have analyzed the chemical properties of air pollution over the Huabei region in Eastern China, using the measurement data obtained during the IPAC-NC campaign in spring 2006. Huabei includes two megacities, i.e., Beijing and Tianjin, and several large industrial areas, e.g., Tangshan, Shijiazhuang and Taiyuan. High pollution emissions, together with the meteorological conditions that favor local convergence, result in the accumulation of pollutants in the lower atmosphere over the core area of Huabei. In addition to high concentrations of gaseous pollutants and haze particles, we deduce high levels of  $\text{HO}_x$  radicals and active photochemistry in the lower atmosphere over the region, leading to the efficient formation of ozone and secondary aerosols. The results thus indicate that the lower atmosphere over Huabei is not only highly polluted but also acts as an oxidation pool over this part of China.

During IPAC-NC, daytime mean near-surface concentrations and standard deviations of the primary gaseous pollutants  $\text{SO}_2$ ,  $\text{NO}$ ,  $\text{NO}_x$ ,  $\text{CO}$ , and NMHCs were  $24.7 \pm 20.9$  ppbv,  $8.4 \pm 15.6$  ppbv,  $29.4 \pm 23.1$  ppbv,  $1.5 \pm 1.0$  ppmv, and  $55.1 \pm 45.7$  ppbv, respectively, in the polluted rural area of Huabei. Airborne measurements show that throughout the PBL and in the lower free troposphere the levels of these pollutants were also high. We observed widespread and high  $\text{SO}_2$  mixing ratios of 20–40 ppbv at 0.5–1.5 km and 10–30 ppbv at 1.5–3.0 km altitude. Over the most highly polluted areas  $\text{SO}_2$  reached up to 60–100 ppbv in the PBL, much higher than at the surface owing to the predominantly elevated sources by industrial stacks. Average CO during the

## The IPAC-NC field campaign

J. Z. Ma et al.

Title Page

Abstract

Introduction

Conclusions

References

Tables

Figures

◀

▶

◀

▶

Back

Close

Full Screen / Esc

Printer-friendly Version

Interactive Discussion



**The IPAC-NC field campaign**

J. Z. Ma et al.

Title Page

Abstract

Introduction

Conclusions

References

Tables

Figures

◀

▶

◀

▶

Back

Close

Full Screen / Esc

Printer-friendly Version

Interactive Discussion



campaign period was  $\sim 0.7$  ppmv at 0.5–1.5 km altitude, and very high CO mixing ratios of  $\sim 1$  ppmv were observed during some flights, and even higher levels at the surface. The  $\text{SO}_2$  in the lower atmosphere over Huabei observed during IPAC-NC was a few times higher than measured over an area in the northeastern part of China during April 2005, i.e. outside of the central pollution pool, and an order of magnitude higher than those over the NE United States (Dickerson et al., 2007).

Our chemical box-model simulations, constrained by the measurements, suggest a maximum in the vertical profiles of OH and  $\text{HO}_2$  at an altitude of  $\sim 1$  km over the polluted area of Huabei. The peak OH concentration is estimated to be  $6.9 \times 10^6$  molecules  $\text{cm}^{-3}$  ( $\sim 0.29$  pptv), substantially higher than the surface level of  $5.4 \times 10^6$  molecules  $\text{cm}^{-3}$  ( $\sim 0.22$  pptv). It is shown that the combined effective photolysis of ozone and the recycling of radicals in the photochemistry of  $\text{NO}_2$ , CO, VOC and  $\text{SO}_2$  lead to high levels of  $\text{HO}_x$  radicals in the lower atmosphere over Huabei. At the surface, high concentrations of  $\text{NO}_2$  suppress the recycling of  $\text{HO}_x$  radicals by the termination reaction  $\text{NO}_2 + \text{OH}$ . In contrast, at higher altitudes within the PBL, CO and  $\text{SO}_2$  more effectively compete with relatively less  $\text{NO}_2$  to react with OH, recycling  $\text{HO}_2$  more efficiently without a loss of total  $\text{HO}_x$ . OH levels in the lower atmosphere over Huabei appear to be similar to those over the Gulf of Mexico and 2–3 times higher than over the subtropical Pacific (Singh et al., 2009). The relatively high OH concentrations in the lower atmosphere over Huabei indicate that primary pollutants are efficiently oxidized before being transported to the Pacific and towards the North American continent.

At the high  $\text{NO}_x$  levels over Huabei photochemical ozone formation is limited by the radical abundance and the oxidation rates of CO and VOCs. We estimate that the contribution of VOCs to instantaneous ozone production over Huabei,  $P(\text{O}_3)$ , is  $\sim 85\%$  near the surface and 60–75% at higher altitudes in the PBL and lower free troposphere. The oxidation of CO contributes about 14% to  $P(\text{O}_3)$  at the surface and 12–25% aloft. Interestingly, we find that the oxidation of  $\text{SO}_2$  also contributes significantly (up to  $\sim 13\%$  or  $2.0$  ppbv  $\text{h}^{-1}$  at 0.8 km) to ozone production. The estimated  $P(\text{O}_3)$  rate at the surface during IPAC-NC is  $48$  ppbv  $\text{h}^{-1}$ , comparable to the high maximum value of  $50$  ppbv  $\text{h}^{-1}$

**The IPAC-NC field campaign**

J. Z. Ma et al.

Title Page

Abstract

Introduction

Conclusions

References

Tables

Figures

◀

▶

◀

▶

Back

Close

Full Screen / Esc

Printer-friendly Version

Interactive Discussion



at a suburban site of Beijing reported by Lu et al. (2010). Ozone production in the PBL over Huabei (e.g.,  $16 \text{ ppbv h}^{-1}$  at 0.8 km) appears to be much higher than that over the polluted Asian continent during INTEX-B ( $>5 \text{ ppbv d}^{-1}$  at 800 hPa), derived from simulations by Zhang et al. (2008b) using a global model. Note that the IPAC-NC and INTEX-B campaigns were performed in the same period, i.e., spring 2006.

The high OH levels tend to promote the formation of semi- and low-volatile species such as inorganic and organic acids through the oxidation of  $\text{SO}_2$ ,  $\text{NO}_2$  and VOCs. In spring, the atmospheric load of primary aerosols over Huabei is very high due to strong emissions from both natural and anthropogenic sources (e.g., dust and black carbon), providing a large surface area for the condensation of these oxidation products. The condensation rate of sulfuric acid is estimated to be  $2\text{--}8 \mu\text{g cm}^{-3} \text{ h}^{-1}$  during IPAC-NC, with a maximum at about 0.8 km altitude. The calculated condensation potential of secondary organics was much lower, with a maximum of  $\sim 0.5 \mu\text{g cm}^{-3} \text{ h}^{-1}$  at the surface, though this is probably a lower limit. Our analyses nevertheless underscore the importance of ozone and radical chemistry for the formation of secondary organic aerosols. The interactions between pollution emissions, photochemistry, the atmospheric oxidation capacity and haze formation are intricate and require continued investigations.

*Acknowledgements.* This work was supported by the NSFC projects 40433008, 40775073 & 41075095 and the ERC project C8. We are grateful to Xiaobin Wang and Jian Sun of CAMS, Mingzhi Xu and Baohui Yin of CRAES, Ruijun Jin of TJWMO, and other staff and graduate students for participating in the IPAC-NC campaign 2006. We thank Chuenyu Chan of PolyU/SYSU, Xiaobin Xu, Xiangdong Zheng and Hongbing Cheng of CAMS, and Sihua Lu and Min Shao of PKU for their helps on VOC sampling and analysis. We also thank Benedikt Steil of the MPIC for providing the EMAC model results. We acknowledge the open access of tropospheric  $\text{NO}_2$  column data from the OMI sensor from <http://www.temis.nl>. This paper is dedicated to Wei Wang for his great contributions to atmospheric chemistry research especially aircraft measurements of air pollution in China.

## References

- Akimoto, H.: Global air quality and pollution, *Science*, 302, 1716–1719, doi:10.1126/science.1092666, 2003.
- Ammann, M., Kalberer, M., Jost, D. T., Tobler, L., Rossler, E., Pignatelli, D., Gaggeler, H. W., and Baltensperger, U.: Heterogeneous production of nitrous acid on soot in polluted air masses, *Nature*, 395, 157–160, 1998.
- An, J. L., Zhang, W., and Qu, Y.: Impacts of a strong cold front on concentrations of HONO, HCHO, O<sub>3</sub>, and NO<sub>2</sub> in the heavy traffic urban area of Beijing, *Atmos. Environ.*, 43, 3454–3459, doi:10.1016/j.atmosenv.2009.04.052, 2009.
- Apel, E. C., Emmons, L. K., Karl, T., Flocke, F., Hills, A. J., Madronich, S., Lee-Taylor, J., Fried, A., Weibring, P., Walega, J., Richter, D., Tie, X., Mauldin, L., Campos, T., Weinheimer, A., Knapp, D., Sive, B., Kleinman, L., Springston, S., Zaveri, R., Ortega, J., Voss, P., Blake, D., Baker, A., Warneke, C., Welsh-Bon, D., de Gouw, J., Zheng, J., Zhang, R., Rudolph, J., Junkermann, W., and Riemer, D. D.: Chemical evolution of volatile organic compounds in the outflow of the Mexico City Metropolitan area, *Atmos. Chem. Phys.*, 10, 2353–2375, doi:10.5194/acp-10-2353-2010, 2010.
- Barletta, B., Meinardi, S., Simpson, I. J., Atlas, E. L., Beyersdorf, A. J., Baker, A. K., Blake, N. J., Yang, M., Midyett, J. R., Novak, B. J., McKeachie, R. J., Fuelberg, H. E., Sachse, G. W., Avery, M. A., Campos, T., Weinheimer, A. J., Rowland, F. S., and Blake, D. R.: Characterization of volatile organic compounds (VOCs) in Asian and north American pollution plumes during INTEX-B: identification of specific Chinese air mass tracers, *Atmos. Chem. Phys.*, 9, 5371–5388, doi:10.5194/acp-9-5371-2009, 2009.
- Boersma, K. F., Eskes, H. J., Veefkind, J. P., Brinksma, E. J., van der A, R. J., Sneep, M., van den Oord, G. H. J., Levelt, P. F., Stammes, P., Gleason, J. F., and Bucsela, E. J.: Near-real time retrieval of tropospheric NO<sub>2</sub> from OMI, *Atmos. Chem. Phys.*, 7, 2103–2118, doi:10.5194/acp-7-2103-2007, 2007.
- Boersma, K. F., Jacob, D. J., Eskes, H. J., Pinder, R. W., Wang, J., and van der A, R. J.: Intercomparison of SCIAMACHY and OMI tropospheric NO<sub>2</sub> columns: Observing the diurnal evolution of chemistry and emissions from space, *J. Geophys. Res.*, 113, doi:10.1029/2007jd008816, 2008.
- Chan, C. K. and Yao, X.: Air pollution in mega cities in China, *Atmos. Environ.*, 42, 1–42, 2008.
- Chen, Y., Zhao, C., Zhang, Q., Deng, Z., Huang, M., and Ma, X.: Aircraft study

## The IPAC-NC field campaign

J. Z. Ma et al.

Title Page

Abstract

Introduction

Conclusions

References

Tables

Figures

◀

▶

◀

▶

Back

Close

Full Screen / Esc

Printer-friendly Version

Interactive Discussion



**The IPAC-NC field campaign**

J. Z. Ma et al.

Title Page

Abstract

Introduction

Conclusions

References

Tables

Figures

◀

▶

◀

▶

Back

Close

Full Screen / Esc

Printer-friendly Version

Interactive Discussion



of Mountain Chimney Effect of Beijing, China, *J. Geophys. Res.*, 114, D08306, doi:10.1029/2008jd010610, 2009.

Cheng, H. and Wang, M.: Difference in Nonmethane Hydrocarbons (NMHCs) between Urban and Rural Atmospheres, *Meteorol. Sci. Technol.*, 38, 668–672, 2010 (in Chinese).

5 Commane, R., Floquet, C. F. A., Ingham, T., Stone, D., Evans, M. J., and Heard, D. E.: Observations of OH and HO<sub>2</sub> radicals over West Africa, *Atmos. Chem. Phys.*, 10, 8783–8801, doi:10.5194/acp-10-8783-2010, 2010.

Cooper, O. R., Parrish, D. D., Stohl, A., Trainer, M., Nédélec, P., Thouret, V., Cammas, J. P., Oltmans, S. J., Johnson, B. J., Tarasick, D., Leblanc, T., McDermid, I. S., Jaffe, D., Gao, R.,  
10 Stith, J., Ryerson, T., Aikin, K., Campos, T., Weinheimer, A., and Avery, M. A.: Increasing springtime ozone mixing ratios in the free troposphere over Western North America, *Nature*, 463, 344–348, 2010.

Crutzen, P. R. and Andreae, M. O.: Biomass burning in the tropics: Impact on atmospheric chemistry and biogeochemical cycles, *Science*, 250, 1669–1678, 1990.

15 de Gouw, J. A., Middlebrook, A. M., Warneke, C., Ahmadov, R., Atlas, E. L., Bahreini, R., Blake, D. R., Brock, C. A., Brioude, J., Fahey, D. W., Fehsenfeld, F. C., Holloway, J. S., Le Henaff, M., Lueb, R. A., McKeen, S. A., Meagher, J. F., Murphy, D. M., Paris, C., Parrish, D. D., Perring, A. E., Pollack, I. B., Ravishankara, A. R., Robinson, A. L., Ryerson, T. B., Schwarz, J. P., Spackman, J. R., Srinivasan, A., and Watts, L. A.: Organic aerosol formation downwind from the deepwater horizon oil spill, *Science*, 331, 1295–1299, doi:10.1126/science.1200320, 2011.

de Reus, M., Fischer, H., Sander, R., Gros, V., Kormann, R., Salisbury, G., Van Dingenen, R., Williams, J., Zöllner, M., and Lelieveld, J.: Observations and model calculations of trace gas scavenging in a dense Saharan dust plume during MINATROC, *Atmos. Chem. Phys.*, 5, 1787–1803, doi:10.5194/acp-5-1787-2005, 2005.

25 Dickerson, R. R., Li, C., Li, Z., Marufu, L. T., Stehr, J. W., McClure, B., Krotkov, N., Chen, H., Wang, P., Xia, X., Ban, X., Gong, F., Yuan, J., and Yang, J.: Aircraft observations of dust and pollutants over Northeast China: Insight into the meteorological mechanisms of transport, *J. Geophys. Res.*, 112, 10.1029/2007jd008999, 2007.

30 Ding, A. J., Wang, T., Thouret, V., Cammas, J.-P., and Nédélec, P.: Tropospheric ozone climatology over Beijing: analysis of aircraft data from the MOZAIC program, *Atmos. Chem. Phys.*, 8, 1–13, doi:10.5194/acp-8-1-2008, 2008.

Ehhalt, D. H.: Photooxidation of trace gases in the troposphere Plenary Lecture, *Phys. Chem.*

**The IPAC-NC field campaign**

J. Z. Ma et al.

Title Page

Abstract

Introduction

Conclusions

References

Tables

Figures

◀

▶

◀

▶

Back

Close

Full Screen / Esc

Printer-friendly Version

Interactive Discussion



Chem. Phys., 1, 5401–5408, 1999.

Farina, S. C., Adams, P. J., and Pandis, S. N.: Modeling global secondary organic aerosol formation and processing with the volatility basis set: Implications for anthropogenic secondary organic aerosol, *J. Geophys. Res.*, 115, D09202, 10.1029/2009jd013046, 2010.

5 Fiedler, V., Nau, R., Ludmann, S., Arnold, F., Schlager, H., and Stohl, A.: East Asian SO<sub>2</sub> pollution plume over Europe – Part 1: Airborne trace gas measurements and source identification by particle dispersion model simulations, *Atmos. Chem. Phys.*, 9, 4717–4728, doi:10.5194/acp-9-4717-2009, 2009.

10 Geng, F. H., Tie, X. X., Xu, J. M., Zhou, G. Q., Peng, L., Gao, W., Tang, X., and Zhao, C. S.: Characterizations of ozone, NO<sub>x</sub>, and VOCs measured in Shanghai, China, *Atmos. Environ.*, 42, 6873–6883, 10.1016/j.atmosenv.2008.05.045, 2008.

Gurjar, B. R., Butler, T. M., Lawrence, M. G., and Lelieveld, J.: Evaluation of emissions and air quality in megacities, *Atmos. Environ.*, 42, 1593–1606, 2008.

15 Hatakeyama, S., Takami, A., Wang, W., and Tang, D.: Aerial observation of air pollutants and aerosols over Bo Hai, China, *Atmos. Environ.*, 39, 5893–5898, 2005.

Hocking, W. K., Carey-Smith, T., Tarasick, D. W., Argall, P. S., Strong, K., Rochon, Y., Zawadzki, I., and Taylor, P. A.: Detection of stratospheric ozone intrusions by windprofiler radars, *Nature*, 450, 281–284, [http://www.nature.com/nature/journal/v450/n7167/supinfo/nature06312\\_S1.html](http://www.nature.com/nature/journal/v450/n7167/supinfo/nature06312_S1.html), 2007.

20 Hofzumahaus, A., Rohrer, F., Lu, K., Bohn, B., Brauers, T., Chang, C.-C., Fuchs, H., Holland, F., Kita, K., Kondo, Y., Li, X., Lou, S., Shao, M., Zeng, L., Wahner, A., and Zhang, Y.: Amplified trace gas removal in the troposphere, *Science*, 324, 1702–1704, 10.1126/science.1164566, 2009.

25 Jacob, D. J., Crawford, J. H., Kleb, M. M., Connors, V. S., Bendura, R. J., Raper, J. L., Sachse, G. W., Gille, J. C., Emmons, L., and Heald, C. L.: Transport and Chemical Evolution over the Pacific (TRACE-P) aircraft mission: Design, execution, and first results, *J. Geophys. Res.*, 108, 10.1029/2002jd003276, 2003.

30 Jimenez, J. L., Canagaratna, M. R., Donahue, N. M., Prevot, A. S. H., Zhang, Q., Kroll, J. H., DeCarlo, P. F., Allan, J. D., Coe, H., Ng, N. L., Aiken, A. C., Docherty, K. S., Ulbrich, I. M., Grieshop, A. P., Robinson, A. L., Duplissy, J., Smith, J. D., Wilson, K. R., Lanz, V. A., Hueglin, C., Sun, Y. L., Tian, J., Laaksonen, A., Raatikainen, T., Rautiainen, J., Vaattovaara, P., Ehn, M., Kulmala, M., Tomlinson, J. M., Collins, D. R., Cubison, M. J., E., Dunlea, J., Huffman, J. A., Onasch, T. B., Alfarra, M. R., Williams, P. I., Bower, K., Kondo, Y.,

**The IPAC-NC field campaign**

J. Z. Ma et al.

Title Page

Abstract

Introduction

Conclusions

References

Tables

Figures

◀

▶

◀

▶

Back

Close

Full Screen / Esc

Printer-friendly Version

Interactive Discussion



Schneider, J., Drewnick, F., Borrmann, S., Weimer, S., Demerjian, K., Salcedo, D., Cottrell, L., Griffin, R., Takami, A., Miyoshi, T., Hatakeyama, S., Shimono, A., Sun, J. Y., Zhang, Y. M., Dzepina, K., Kimmel, J. R., Sueper, D., Jayne, J. T., Herndon, S. C., Trimborn, A. M., Williams, L. R., Wood, E. C., Middlebrook, A. M., Kolb, C. E., Baltensperger, U., and Worsnop, D. R.: Evolution of organic aerosols in the atmosphere, *Science*, 326, 1525–1529, 10.1126/science.1180353, 2009.

Jöckel, P., Tost, H., Pozzer, A., Brühl, C., Buchholz, J., Ganzeveld, L., Hoor, P., Kerckweg, A., Lawrence, M. G., Sander, R., Steil, B., Stiller, G., Tanarhte, M., Taraborrelli, D., van Aardenne, J., and Lelieveld, J.: The atmospheric chemistry general circulation model ECHAM5/MESSy1: consistent simulation of ozone from the surface to the mesosphere, *Atmos. Chem. Phys.*, 6, 5067–5104, doi:10.5194/acp-6-5067-2006, 2006.

Kanakidou, M., Mihalopoulos, N., Kindap, T., Im, U., Vrekoussis, M., Gerasopoulos, E., Dermizaki, E., Unal, A., Koçak, M., Markakis, K., Melas, D., Kouvarakis, G., Youssef, A. F., Richter, A., Hatzianastassiou, N., Hilboll, A., Ebojje, F., Wittrock, F., von Savigny, C., Burrows, J. P., Ladstaetter-Weissenmayer, A., and Moubasher, H.: Megacities as hot spots of air pollution in the East Mediterranean, *Atmos. Environ.*, 45, 1223–1235, 2011.

Kanaya, Y., Pochanart, P., Liu, Y., Li, J., Tanimoto, H., Kato, S., Suthawaree, J., Inomata, S., Taketani, F., Okuzawa, K., Kawamura, K., Akimoto, H., and Wang, Z. F.: Rates and regimes of photochemical ozone production over Central East China in June 2006: a box model analysis using comprehensive measurements of ozone precursors, *Atmos. Chem. Phys.*, 9, 7711–7723, doi:10.5194/acp-9-7711-2009, 2009.

Kleinman, L. I., Daum, P. H., Imre, D. G., Lee, J. H., Lee, Y.-N., Nunnermacker, L. J., Springston, S. R., Weinstein-Lloyd, J., and Newman, L.: Ozone production in the New York City urban plume, *J. Geophys. Res.*, 105, 14495–14511, 10.1029/2000jd900011, 2000.

Kleinman, L. I., Daum, P. H., Lee, Y. N., Nunnermacker, L. J., Springston, S. R., Weinstein-Lloyd, J., and Rudolph, J.: A comparative study of ozone production in five US metropolitan areas, *J. Geophys. Res.*, 110, D02301, 10.1029/2004jd005096, 2005.

Kubistin, D., Harder, H., Martinez, M., Rudolf, M., Sander, R., Bozem, H., Eerdekens, G., Fischer, H., Gurk, C., Klüpfel, T., Königstedt, R., Parchatka, U., Schiller, C. L., Stickler, A., Taraborrelli, D., Williams, J., and Lelieveld, J.: Hydroxyl radicals in the tropical troposphere over the Suriname rainforest: comparison of measurements with the box model MECCA, *Atmos. Chem. Phys.*, 10, 9705–9728, doi:10.5194/acp-10-9705-2010, 2010.

Kuhn, U., Ganzeveld, L., Thielmann, A., Dindorf, T., Schebeske, G., Welling, M., Sciare, J.,

**The IPAC-NC field campaign**

J. Z. Ma et al.

Title Page

Abstract

Introduction

Conclusions

References

Tables

Figures

◀

▶

◀

▶

Back

Close

Full Screen / Esc

Printer-friendly Version

Interactive Discussion



Roberts, G., Meixner, F. X., Kesselmeier, J., Lelieveld, J., Kolle, O., Ciccioli, P., Lloyd, J., Trentmann, J., Artaxo, P., and Andreae, M. O.: Impact of Manaus City on the Amazon Green Ocean atmosphere: ozone production, precursor sensitivity and aerosol load, *Atmos. Chem. Phys.*, 10, 9251–9282, doi:10.5194/acp-10-9251-2010, 2010.

5 Kulmala, M.: ATMOSPHERIC SCIENCE: How particles nucleate and grow, *Science*, 302, 1000–1001, 10.1126/science.1090848, 2003.

Lawrence, M. G., Butler, T. M., Steinkamp, J., Gurjar, B. R., and Lelieveld, J.: Regional pollution potentials of megacities and other major population centers, *Atmos. Chem. Phys.*, 7, 3969–3987, doi:10.5194/acp-7-3969-2007, 2007.

10 Lawrence, M. G. and Lelieveld, J.: Atmospheric pollutant outflow from Southern Asia: a review, *Atmos. Chem. Phys.*, 10, 11017–11096, doi:10.5194/acp-10-11017-2010, 2010.

Lelieveld, J.: Atmospheric chemistry: A missing sink for radicals, *Nature*, 466, 925–926, 2010.

Lelieveld, J., Berresheim, H., Borrmann, S., Crutzen, P. J., Dentener, F. J., Fischer, H., Feichter, J., Flatau, P. J., Heland, J., Holzinger, R., Korrman, R., Lawrence, M. G.,  
15 Levin, Z., Markowicz, K. M., Mihalopoulos, N., Minikin, A., Ramanathan, V., de Reus, M., Roelofs, G. J., Scheeren, H. A., Sciare, J., Schlager, H., Schultz, M., Siegmund, P., Steil, B., Stephanou, E. G., Stier, P., Traub, M., Warneke, C., Williams, J., and Ziereis, H.: Global air pollution crossroads over the Mediterranean, *Science*, 298, 794–799, 10.1126/science.1075457, 2002a.

20 Lelieveld, J., Peters, W., Dentener, F. J., and Krol, M. C.: Stability of tropospheric hydroxyl chemistry, *J. Geophys. Res.*, 107, 4715, 10.1029/2002jd002272, 2002b.

Lelieveld, J., Butler, T. M., Crowley, J. N., Dillon, T. J., Fischer, H., Ganzeveld, L., Harder, H., Lawrence, M. G., Martinez, M., Taraborrelli, D., and Williams, J.: Atmospheric oxidation capacity sustained by a tropical forest, *Nature*, 452, 737–740, 2008.

25 Lelieveld, J., Hoor, P., Jöckel, P., Pozzer, A., Hadjinicolaou, P., Cammas, J.-P., and Beirle, S.: Severe ozone air pollution in the Persian Gulf region, *Atmos. Chem. Phys.*, 9, 1393–1406, doi:10.5194/acp-9-1393-2009, 2009.

Levy, H. I.: Normal atmosphere: large radical and formaldehyde concentrations predicted, *Science*, 173, 141–143, 1971.

30 Li, C., Marufu, L. T., Dickerson, R. R., Li, Z., Wen, T., Wang, Y., Wang, P., Chen, H., and Stehr, J. W.: In situ measurements of trace gases and aerosol optical properties at a rural site in Northern China during East Asian Study of Tropospheric Aerosols: An International Regional Experiment 2005, *J. Geophys. Res.*, 112, D22S04, 10.1029/2006jd007592, 2007.

- Lin, W., Xu, X., Zhang, X., and Tang, J.: Contributions of pollutants from North China Plain to surface ozone at the Shangdianzi GAW Station, *Atmos. Chem. Phys.*, 8, 5889–5898, doi:10.5194/acp-8-5889-2008, 2008.
- Lin, W., Xu, X., Ge, B., and Zhang, X.: Characteristics of gaseous pollutants at Gucheng, a rural site southwest of Beijing, *J. Geophys. Res.*, 114, 10.1029/2008jd010339, 2009.
- Liu, S., Trainer, M., Fehsenfeld, F., Parrish, D., Williams, E., Fahey, D., Hübler, G., and Murphy, P.: Ozone production in the rural troposphere and the implications for regional and global ozone distributions, *J. Geophys. Res.*, 92, 4191–4207, 1987.
- Lou, S., Holland, F., Rohrer, F., Lu, K., Bohn, B., Brauers, T., Chang, C.C., Fuchs, H., Häsel, R., Kita, K., Kondo, Y., Li, X., Shao, M., Zeng, L., Wahner, A., Zhang, Y., Wang, W., and Hofzumahaus, A.: Atmospheric OH reactivities in the Pearl River Delta China in summer 2006: measurement and model results, *Atmos. Chem. Phys.*, 10, 11243–11260, doi:10.5194/acp-10-11243-2010, 2010.
- Lu, K., Zhang, Y., Su, H., Brauers, T., Chou, C. C., Hofzumahaus, A., Liu, S. C., Kita, K., Kondo, Y., Shao, M., Wahner, A., Wang, J., Wang, X., and Zhu, T.: Oxidant ( $O_3 + NO_2$ ) production processes and formation regimes in Beijing, *J. Geophys. Res.*, 115, D07303, 10.1029/2009jd012714, 2010.
- Ma, J. and Weele, M. v.: Effect of stratospheric ozone depletion on the net production of ozone in polluted rural areas, *Chemosphere – Global Change Science*, 2, 23–37, 2000.
- Ma, J., Liu, H., and Hauglustaine, D.: Summertime tropospheric ozone over China simulated with a regional chemical transport model 1. Model description and evaluation, *J. Geophys. Res.*, 107, 4660, 10.1029/2001jd001354, 2002a.
- Ma, J., Tang, J., Zhou, X., and Zhang, X.: Estimates of the chemical budget for ozone at Waliguan Observatory, *J. Atmos. Chem.*, 41, 21–48, 10.1023/A:1013892308983 2002b.
- Ma, J., Zhou, X., and Hauglustaine, D.: Summertime tropospheric ozone over China simulated with a regional chemical transport model 2. Source contributions and budget, *J. Geophys. Res.*, 107, 4612, 10.1029/2001jd001355, 2002c.
- Ma, J., Richter, A., Burrows, J. P., Nüß, H., and van Aardenne, J. A.: Comparison of model-simulated tropospheric  $NO_2$  over China with GOME-satellite data, *Atmos. Environ.*, 40, 593–604, 2006.
- Ma, J., Chen, Y., Wang, W., Yan, P., Liu, H., Yang, S., Hu, Z., and Lelieveld, J.: Strong air pollution causes widespread haze-clouds over China, *J. Geophys. Res.*, 115, D18204, 10.1029/2009jd013065, 2010.

**The IPAC-NC field campaign**

J. Z. Ma et al.

Title Page

Abstract

Introduction

Conclusions

References

Tables

Figures

◀

▶

◀

▶

Back

Close

Full Screen / Esc

Printer-friendly Version

Interactive Discussion



**The IPAC-NC field campaign**

J. Z. Ma et al.

Title Page

Abstract

Introduction

Conclusions

References

Tables

Figures

◀

▶

◀

▶

Back

Close

Full Screen / Esc

Printer-friendly Version

Interactive Discussion



- Madronich, S.: Photodissociation in the atmosphere: 1. Actinic flux and the effects of ground reflections and clouds, *J. Geophys. Res.*, 92, 9740–9752, 1987.
- Madronich, S. and Calvert, J. G.: The NCAR master mechanism of the gas-phase chemistry- Version 2.0, The National Center for Atmospheric Research, Boulder, Colorado. Rep. NCAR/TN-333+STR., 1989.
- 5 Madronich, S. and Calvert, J. G.: Permutation reactions of organic peroxy radicals in the troposphere, *J. Geophys. Res.*, 95, 5697–5715, 1990.
- Mao, J., Ren, X., Brune, W. H., Olson, J. R., Crawford, J. H., Fried, A., Huey, L. G., Cohen, R. C., Heikes, B., Singh, H. B., Blake, D. R., Sachse, G. W., Diskin, G. S., Hall, S. R., and Shetter, R. E.: Airborne measurement of OH reactivity during INTEX-B, *Atmos. Chem. Phys.*, 9, 163–173, doi:10.5194/acp-9-163-2009, 2009.
- 10 Mao, J., Jacob, D. J., Evans, M. J., Olson, J. R., Ren, X., Brune, W. H., Clair, J. M. St., Crounse, J. D., Spencer, K. M., Beaver, M. R., Wennberg, P. O., Cubison, M. J., Jimenez, J. L., Fried, A., Weibring, P., Walega, J. G., Hall, S. R., Weinheimer, A. J., Cohen, R. C., Chen, G., Crawford, J. H., McNaughton, C., Clarke, A. D., Jaeglé, L., Fisher, J. A., Yantosca, R. M., Le Sager, P., and Carouge, C.: Chemistry of hydrogen oxide radicals ( $\text{HO}_x$ ) in the Arctic troposphere in spring, *Atmos. Chem. Phys.*, 10, 5823–5838, doi:10.5194/acp-10-5823-2010, 2010.
- 15 Martinez, M., Harder, H., Kubistin, D., Rudolf, M., Bozem, H., Eerdeken, G., Fischer, H., Klüpfel, T., Gurk, C., Königstedt, R., Parchatka, U., Schiller, C. L., Stickler, A., Williams, J., and Lelieveld, J.: Hydroxyl radicals in the tropical troposphere over the Suriname rainforest: airborne measurements, *Atmos. Chem. Phys.*, 10, 3759–3773, doi:10.5194/acp-10-3759-2010, 2010.
- 20 Meng, Z. Y., Xu, X. B., Yan, P., Ding, G. A., Tang, J., Lin, W. L., Xu, X. D., and Wang, S. F.: Characteristics of trace gaseous pollutants at a regional background station in Northern China, *Atmos. Chem. Phys.*, 9, 927–936, doi:10.5194/acp-9-927-2009, 2009.
- Mijling, B., van der A, R. J., Boersma, K. F., Van Roozendaal, M., De Smedt, I., and Kelder, H. M.: Reductions of  $\text{NO}_2$  detected from space during the 2008 Beijing Olympic Games, *Geophys. Res. Lett.*, 36, 10.1029/2009gl038943, 2009.
- 30 Molina, M. J. and Molina, L. T.: Megacities and atmospheric pollution, *J. Air Waste Manage.*, 54, 644–680, 2004.
- Molina, L. T., Kolb, C. E., de Foy, B., Lamb, B. K., Brune, W. H., Jimenez, J. L., Ramos- Villegas, R., Sarmiento, J., Paramo-Figueroa, V. H., Cardenas, B., Gutierrez-Avedoy, V., and

**The IPAC-NC field campaign**

J. Z. Ma et al.

Title Page

Abstract

Introduction

Conclusions

References

Tables

Figures

◀

▶

◀

▶

Back

Close

Full Screen / Esc

Printer-friendly Version

Interactive Discussion



- Molina, M. J.: Air quality in North America's most populous city – overview of the MCMA-2003 campaign, *Atmos. Chem. Phys.*, 7, 2447–2473, doi:10.5194/acp-7-2447-2007, 2007.
- Molina, L. T., Madronich, S., Gaffney, J. S., Apel, E., de Foy, B., Fast, J., Ferrare, R., Hernandez, S., Jimenez, J. L., Lamb, B., Osornio-Vargas, A. R., Russell, P., Schauer, J. J., Stevens, P. S., Volkamer, R., and Zavala, M.: An overview of the MILAGRO 2006 Campaign: Mexico City emissions and their transport and transformation, *Atmos. Chem. Phys.*, 10, 8697–8760, doi:10.5194/acp-10-8697-2010, 2010.
- Pan, X. L., Yan, P., Tang, J., Ma, J. Z., Wang, Z. F., Gbaguidi, A., and Sun, Y. L.: Observational study of influence of aerosol hygroscopic growth on scattering coefficient over rural area near Beijing mega-city, *Atmos. Chem. Phys.*, 9, 7519–7530, doi:10.5194/acp-9-7519-2009, 2009.
- Pope, C. A. and Dockery, D. W.: Health effects of fine particulate air pollution: lines that connect, *J. Air Waste Manage. Assoc.*, 56, 709–742, 2006.
- Ramanathan, V., Chung, C., Kim, D., Bettge, T., Buja, L., Kiehl, J. T., Washington, W. M., Fu, Q., Sikka, D. R., and Wild, M.: Atmospheric brown clouds: impacts on South Asian climate and hydrological cycle, *Proc. Natl. Acad. Sci. USA*, 102, 5326–5333, doi:10.1073/pnas.0500656102, 2005.
- Ren, X., Harder, H., Martinez, M., Leshner, R. L., Olinger, A., Shirley, T., Adams, J., Simpasa, J. B., and Brune, W. H.: HO<sub>x</sub> concentrations and OH reactivity observations in New York City during PMTACS-NY2001, *Atmos. Environ.*, 37, 3627–3637, 2003.
- Richter, A., Burrows, J. P., Nusz, H., Granier, C., and Niemeier, U.: Increase in tropospheric nitrogen dioxide over China observed from space, *Nature*, 437, 129–132, [http://www.nature.com/nature/journal/v437/n7055/supinfo/nature04092\\_S1.html](http://www.nature.com/nature/journal/v437/n7055/supinfo/nature04092_S1.html), 2005.
- Robinson, A. L., Donahue, N. M., Shrivastava, M. K., Weitkamp, E. A., Sage, A. M., Grieshop, A. P., Lane, T. E., Pierce, J. R., and Pandis, S. N.: Rethinking organic aerosols: Semivolatile emissions and photochemical aging, *Science*, 315, 1259–1262, 10.1126/science.1133061, 2007.
- Rohrer, F. and Berresheim, H.: Strong correlation between levels of tropospheric hydroxyl radicals and solar ultraviolet radiation, *Nature*, 442, 184–187, [http://www.nature.com/nature/journal/v442/n7099/supinfo/nature04924\\_S1.html](http://www.nature.com/nature/journal/v442/n7099/supinfo/nature04924_S1.html), 2006.
- Russo, R. S., Talbot, R. W., Dibb, J. E., Scheuer, E., Seid, G., Jordan, C. E., Fuelberg, H. E., Sachse, G. W., Avery, M. A., Vay, S. A., Blake, D. R., Blake, N. J., Atlas, E., Fried, A., Sandholm, S. T., Tan, D., Singh, H. B., Snow, J., and Heikes, B. G.: Chemical composition of Asian continental outflow over the Western Pacific: Results from Transport and Chemical

## The IPAC-NC field campaign

J. Z. Ma et al.

Title Page

Abstract

Introduction

Conclusions

References

Tables

Figures

◀

▶

◀

▶

Back

Close

Full Screen / Esc

Printer-friendly Version

Interactive Discussion



Evolution over the Pacific (TRACE-P), *J. Geophys. Res.*, 108, 8804, 10.1029/2002jd003184, 2003.

Ryerson, T. B., Trainer, M., Holloway, J. S., Parrish, D. D., Huey, L. G., Sueper, D. T., Frost, G. J., Donnelly, S. G., Schauffler, S., Atlas, E. L., Kuster, W. C., Goldan, P. D., Hubler, G., Meagher, J. F., and Fehsenfeld, F. C.: Observations of ozone formation in power plant plumes and implications for ozone control strategies, *Science*, 292, 719–723, 10.1126/science.1058113, 2001.

Seinfeld, J. H. and Pandis, S. N.: *Atmospheric Chemistry and Physics*, John Wiley and Sons., New York, 1998.

Shao, M., Lu, S., Liu, Y., Xie, X., Chang, C., Huang, S., and Chen, Z.: Volatile organic compounds measured in summer in Beijing and their role in ground-level ozone formation, *J. Geophys. Res.*, 114, 10.1029/2008jd010863, 2009.

Sheehy, P. M., Volkamer, R., Molina, L. T., and Molina, M. J.: Oxidative capacity of the Mexico City atmosphere – Part 2: A RO<sub>x</sub> radical cycling perspective, *Atmos. Chem. Phys.*, 10, 6993–7008, doi:10.5194/acp-10-6993-2010, 2010.

Shirley, T. R., Brune, W. H., Ren, X., Mao, J., Leshner, R., Cardenas, B., Volkamer, R., Molina, L. T., Molina, M. J., Lamb, B., Velasco, E., Jobson, T., and Alexander, M.: Atmospheric oxidation in the Mexico City Metropolitan Area (MCMA) during April 2003, *Atmos. Chem. Phys.*, 6, 2753–2765, doi:10.5194/acp-6-2753-2006, 2006.

Sillman, S.: The relation between ozone, NO<sub>x</sub> and hydrocarbons in urban and polluted rural environments, *Atmos. Environ.*, 33, 1821–1845, 1999.

Singh, H. B., Brune, W. H., Crawford, J. H., Flocke, F., and Jacob, D. J.: Chemistry and transport of pollution over the Gulf of Mexico and the Pacific: spring 2006 INTEX-B campaign overview and first results, *Atmos. Chem. Phys.*, 9, 2301–2318, doi:10.5194/acp-9-2301-2009, 2009.

Sinha, V., Williams, J., Lelieveld, J., Ruuskanen, T. M., Kajos, M. K., Patokoski, J., Hellen, H., Hakola, H., Mogensen, D., Boy, M., Rinne, J., and Kulmala, M.: OH reactivity measurements within a boreal forest: Evidence for unknown reactive emissions, *Environ. Sci. Technol.*, 44, 6614–6620, 10.1021/es101780b, 2010.

Solomon, P., Cowling, E., Hidy, G., and Furiness, C.: Comparison of scientific findings from major ozone field studies in North America and Europe, *Atmos. Environ.*, 34, 1885–1920, 2000.

Stemmler, K., Ammann, M., Donders, C., Kleffmann, J., and George, C.: Photosensitized reduction of nitrogen dioxide on humic acid as a source of nitrous acid, *Nature*, 440, 195–198,

## The IPAC-NC field campaign

J. Z. Ma et al.

Title Page

Abstract

Introduction

Conclusions

References

Tables

Figures

◀

▶

◀

▶

Back

Close

Full Screen / Esc

Printer-friendly Version

Interactive Discussion



- [http://www.nature.com/nature/journal/v440/n7081/suppinfo/nature04603\\_S1.html](http://www.nature.com/nature/journal/v440/n7081/suppinfo/nature04603_S1.html), 2006.
- Stockwell, W. R., Kirchner, F., Kuhn, M., and Seefeld, S.: A new mechanism for regional atmospheric chemistry modeling, *J. Geophys. Res.*, 102, 25847–25879, 10.1029/97jd00849, 1997.
- 5 Su, H., Cheng, Y. F., Shao, M., Gao, D. F., Yu, Z. Y., Zeng, L. M., Slanina, J., Zhang, Y. H., and Wiedensohler, A.: Nitrous acid (HONO) and its daytime sources at a rural site during the 2004 PRIDE-PRD experiment in China, *J. Geophys. Res.-Atmos.*, 113, D14312 10.1029/2007jd009060, 2008.
- 10 Su, H., Cheng, Y., Oswald, R., Behrendt, T., Trebs, I., Meixner, F. X., Andreae, M. O., Cheng, P., Zhang, Y., and Pöschl, U.: Soil nitrite as a source of atmospheric HONO and OH radicals, *Science*, 10.1126/science.1207687, 2011.
- Volkamer, R., Sheehy, P., Molina, L. T., and Molina, M. J.: Oxidative capacity of the Mexico City atmosphere – Part 1: A radical source perspective, *Atmos. Chem. Phys.*, 10, 6969–6991, doi:10.5194/acp-10-6969-2010, 2010.
- 15 Wang, Y., McElroy, M. B., Boersma, K. F., Eskes, H. J., and Veefkind, J. P.: Traffic restrictions associated with the Sino-African summit: Reductions of NO<sub>x</sub> detected from space, *Geophys. Res. Lett.*, 34, L08814, 10.1029/2007gl029326, 2007.
- Wang, W., Ma, J., Hatakeyama, S., Liu, X., Chen, Y., Takami, A., Ren, L., and Geng, C.: Aircraft measurements of vertical ultrafine particles profiles over Northern China coastal areas during dust storms in 2006, *Atmos. Environ.*, 42, 5715–5720, 2008.
- 20 Wang, Y., Hao, J., McElroy, M. B., Munger, J. W., Ma, H., Chen, D., and Nielsen, C. P.: Ozone air quality during the 2008 Beijing Olympics: effectiveness of emission restrictions, *Atmos. Chem. Phys.*, 9, 5237–5251, doi:10.5194/acp-9-5237-2009, 2009.
- Wang, T., Nie, W., Gao, J., Xue, L. K., Gao, X. M., Wang, X. F., Qiu, J., Poon, C. N., Meinardi, S., Blake, D., Wang, S. L., Ding, A. J., Chai, F. H., Zhang, Q. Z., and Wang, W. X.: Air quality during the 2008 Beijing Olympics: secondary pollutants and regional impact, *Atmos. Chem. Phys.*, 10, 7603–7615, doi:10.5194/acp-10-7603-2010, 2010.
- 25 Xu, X. D., Zhou, X. J., and Shi, X. H.: Spatial structure and scale feature of the atmospheric pollution source impact of city agglomeration, *Science in China, Ser. D. Earth Sciences*, 48(Supp. II), 1–24, 2005.
- 30 Yan, P., Tang, J., Huang, J., Mao, J. T., Zhou, X. J., Liu, Q., Wang, Z. F., and Zhou, H. G.: The measurement of aerosol optical properties at a rural site in Northern China, *Atmos. Chem. Phys.*, 8, 2229–2242, doi:10.5194/acp-8-2229-2008, 2008.

**The IPAC-NC field campaign**

J. Z. Ma et al.

Title Page

Abstract

Introduction

Conclusions

References

Tables

Figures

◀

▶

◀

▶

Back

Close

Full Screen / Esc

Printer-friendly Version

Interactive Discussion



- Yu, H., Wang, P. C., Zong, X. M., Li, X., and Lu, D. R.: Change of NO<sub>2</sub> column density over Beijing from satellite measurement during the Beijing 2008 Olympic Games, *Chin. Sci. Bull.*, 55, 308–313, 10.1007/s11434-009-0375-0, 2010.
- Yuan, Z., Lau, A. K. H., Shao, M., Louie, P. K. K., Liu, S. C., and Zhu, T.: Source analysis of volatile organic compounds by positive matrix factorization in urban and rural environments in Beijing, *J. Geophys. Res.*, 114, 10.1029/2008jd011190, 2009.
- Zaveri, R. A., Berkowitz, C. M., Kleinman, L. I., Springston, S. R., Doskey, P. V., Lonnenman, W. A., and Spicer, C. W.: Ozone production efficiency and NO<sub>x</sub> depletion in an urban plume: Interpretation of field observations and implications for evaluating O<sub>3</sub>-NO<sub>x</sub>-VOC sensitivity, *J. Geophys. Res.*, 108, 4436, 10.1029/2002jd003144, 2003.
- Zhang, J., Wang, T., Chameides, W. L., Cardelino, C., Blake, D. R., and Streets, D. G.: Source characteristics of volatile organic compounds during high ozone episodes in Hong Kong, Southern China, *Atmos. Chem. Phys.*, 8, 4983–4996, doi:10.5194/acp-8-4983-2008, 2008a.
- Zhang, L., Jacob, D. J., Boersma, K. F., Jaffe, D. A., Olson, J. R., Bowman, K. W., Worden, J. R., Thompson, A. M., Avery, M. A., Cohen, R. C., Dibb, J. E., Flock, F. M., Fuelberg, H. E., Huey, L. G., McMillan, W. W., Singh, H. B., and Weinheimer, A. J.: Transpacific transport of ozone pollution and the effect of recent Asian emission increases on air quality in North America: an integrated analysis using satellite, aircraft, ozonesonde, and surface observations, *Atmos. Chem. Phys.*, 8, 6117–6136, doi:10.5194/acp-8-6117-2008, 2008b.
- Zhang, Y. H., Hu, M., Zhong, L. J., Wiedensohler, A., Liu, S. C., Andreae, M. O., Wang, W., and Fan, S. J.: Regional Integrated Experiments on Air Quality over Pearl River Delta 2004 (PRIDE-PRD2004): Overview, *Atmos. Environ.*, 42, 6157–6173, 10.1016/j.atmosenv.2008.03.025, 2008c.
- Zhang, Q., Ma, X. C., Tie, X. X., Huang, M. Y., and Zhao, C. S.: Vertical distributions of aerosols under different weather conditions: Analysis of in-situ aircraft measurements in Beijing, China, *Atmos. Environ.*, 43, 5526–5535, 10.1016/j.atmosenv.2009.05.037, 2009a.
- Zhang, Q., Streets, D. G., Carmichael, G. R., He, K. B., Huo, H., Kannari, A., Klimont, Z., Park, I. S., Reddy, S., Fu, J. S., Chen, D., Duan, L., Lei, Y., Wang, L. T., and Yao, Z. L.: Asian emissions in 2006 for the NASA INTEX-B mission, *Atmos. Chem. Phys.*, 9, 5131–5153, doi:10.5194/acp-9-5131-2009, 2009b.
- Zhao, B., Wang, P., Ma, J. Z., Zhu, S., Pozzer, A., and Li, W.: A high-resolution emission inventory of primary pollutants for the Huabei region, China, *Atmos. Chem. Phys. Discuss.*, 11, 20331–20374, doi:10.5194/acpd-11-20331-2011, 2011.

Zhu, S., Butler, T., Sander, R., Ma, J., and Lawrence, M. G.: Impact of dust on tropospheric chemistry over polluted regions: a case study of the Beijing megacity, Atmos. Chem. Phys., 10, 3855–3873, doi:10.5194/acp-10-3855-2010, 2010.

Discussion Paper | Discussion Paper | Discussion Paper | Discussion Paper | Discussion Paper

ACPD

11, 27701–27762, 2011

## The IPAC-NC field campaign

J. Z. Ma et al.

[Title Page](#)

[Abstract](#)

[Introduction](#)

[Conclusions](#)

[References](#)

[Tables](#)

[Figures](#)

[I◀](#)

[▶I](#)

[◀](#)

[▶](#)

[Back](#)

[Close](#)

[Full Screen / Esc](#)

[Printer-friendly Version](#)

[Interactive Discussion](#)



## The IPAC-NC field campaign

J. Z. Ma et al.

**Table 1.** Overview of the aircraft measurements made during IPAC-NC.

Item	Instrument	Temporal resolution	Measurement properties	Invalid flights
SO <sub>2</sub>	TE43C	80 s	DL: 0.1 ppvb	RF02,
CO	TE48C	1 s	DL: 5 ppvb	RF02, RF17, TF2
NO <sub>x</sub>	TE42C	10 s	DL: 0.1 ppvb	RF02, RF07
O <sub>3</sub>	TE49C	20 s	DL: 0.1 ppvb	RF02
VOCs	Canisters	2–4 samples flight <sup>-1</sup>	Alkanes, alkenes, aromatics	TF2
PM <sub>10</sub>	Quartz filters	1–2 samples flight <sup>-1</sup>	Ions, element, EC/OC	TF2
CN	TSI-3020	1 s	SR: >5 nm	RF02, TF2
$N_{1,aer}$	TSI-EEPS-3090	1 s	SR: 5.6–560 nm, 32 bins	RF08–17, TF1–2
$N_{2,aer}$	TSI-APS-3310A	30 s	SR: 0.47–30 μm, 58 bins	TF2
$N_{3,aer}$	PCASP-100X	1 s	SR: 0.1–3.0 μm, 15 bins	RF04
$N_{cld}$	FSSP-100	1 s	SR: 2–47 μm, 15 bins	RF04
$T$	EMM-01	1 s	Accuracy: 0.008 °C	RF02
$T_d$	DP3-D-SH	1 s	Accuracy: 0.1 °C	RF02
GPS	GPS-Global Water	1 s		

$N_{i,aer}$  and  $N_{cld}$ : aerosol and cloud number concentrations, respectively; DL: detect limit; SR: size range. See Table 2 for flight information.

Title Page

Abstract

Introduction

Conclusions

References

Tables

Figures

◀

▶

◀

▶

Back

Close

Full Screen / Esc

Printer-friendly Version

Interactive Discussion



## The IPAC-NC field campaign

J. Z. Ma et al.

**Table 2.** Overview of aircraft flights performed during IPAC-NC.

Flight	Flight description	Flight route pattern	Date in 2006	Take off-Landing Time (UTC)	Flight altitude (m)	Weather condition
TF1	Changzhou-Tianjin	Line	2 Apr	03:30–07:58	2500	Hazy
RF01	Huangzhuang	Circle	9 Apr	01:54–05:50	2800 ~ 400	Cloudy
RF02	Bohai (over sea)	Circle	12 Apr	05:17–10:20	2800 ~ 400	Hazy
RF03	Baodi-Jinghai-Tanggu	Line	13 Apr	11:25–14:34	2500 ~ 1000	Clear
RF04	Guojuzi-Haitiancun (over sea)	Line	15 Apr	11:51–14:43	2000 ~ 1000	Hazy
RF05	Tianjin-Tangshan region	Area	16 Apr	01:52–05:46	2300 ~ 1700	Cloudy
RF06	Bohai (over sea)	Circle	17 Apr	01:56–06:28	2800 ~ 400	Dusty
RF07	Tianjin-Tangshan region	Square	18 Apr	01:58–06:31	2500 ~ 1000	Cloudy
RF08	Jixian-Qingxian	Line	22 Apr	02:10–06:03	2500 ~ 500	Clear
RF09	Tianjin-Tangshan region	Area	26 Apr	01:47–06:52	2700 ~ 1000	Cloudy
RF10	Guojuzi-Haitiancun (over sea)	Line	1 May	01:35–06:16	2000 ~ 500	Hazy
RF11	Yutian-Beidagang	Line	3 May	05:19–08:28	3000 ~ 500	Hazy
RF12	Jixian-Qingxian-Ninghe	Line	4 May	01:48–06:44	2500 ~ 500	Cloudy
RF13	Tianjin North region	Area	7 May	04:45–07:04	3000 ~ 500	Hazy
RF14	Jixian-Qingxian (North)	Line	9 May	08:14–11:04	3100 ~ 2400	Cloudy
RF15	Jixian-Qingxian (South)	Line	11 May	09:24–10:54	3100 ~ 1200	Cloudy
RF16	Tianjin-Tangshan region	Area	12 May	04:21–07:50	2000 ~ 1500	Cloudy
RF17	Tianjin-Tangshan region	Area	13 May	07:02–09:02	2700 ~ 600	Clear
TF2	Tianjin-Changzhou	Line	16 May	01:53–05:34	3000	Clear

Beijing Time is (UTC + 8).

Title Page

Abstract

Introduction

Conclusions

References

Tables

Figures

I◀

▶I

◀

▶

Back

Close

Full Screen / Esc

Printer-friendly Version

Interactive Discussion



**Table 3.** Summary of daytime meteorological parameters and trace gas mixing ratios (mean value plus/minus standard deviation, and median value of the data) observed during IPAC-NC.

Parameter	Surface		0.5–1.5 km altitude		1.5–3 km altitude	
	Mean±Std	Median	Mean±Std	Median	Mean±Std	Median
Temperature (°C)	17.2±6.0	17.6	12.6±5.2	12.1	5.0±6.0	4.3
Relative humidity (%)	41.6±23.4	36.0	56.4±24.5	58.5	49.8±22.2	43.0
SO <sub>2</sub>	24.7±20.9	18.6	37.0±18.7	32.6	26.2±12.9	25.5
NO	8.4±15.6	4.5	2.3±2.0	1.9	1.6±1.0	1.5
NO <sub>x</sub> *	29.4±23.1	23.4	18.7±9.4	16.8	10.6±6.0	8.9
CO (ppmv)	1.5±1.0	1.2	0.67±0.64	0.47	0.23±0.15	0.17
O <sub>3</sub>	49.9±26.3	51.6	41.7±10.8	39.5	41.2±6.2	39.7
O <sub>x</sub>	71.0±22.1	67.9	49.0±11.7	46.4	46.4±6.4	44.8
Ethane	3.12±1.54	2.84	–	–	–	–
Ethylene	2.88±2.00	2.00	–	–	–	–
Propylene	1.61±2.59	1.05	–	–	–	–
Propane	2.23±1.95	1.68	0.25±0.18	0.19	0.15±0.16	0.09
<i>n</i> -Butane	–	–	0.49±0.48	1.05	0.16±0.14	0.11
Isobutane	1.12±1.22	0.69	0.30±0.26	0.21	0.09±0.07	0.05
1-Butene/Isobutene	1.06±3.02	0.00	0.35±0.38	0.28	0.20±0.26	0.07
Pentane	1.85±3.10	0.77	0.23±0.25	0.12	0.07±0.07	0.04
2-Methyl-butane	–	–	0.45±0.51	0.28	0.19±0.25	0.09
Pentene	0.64±1.94	0.00	0.06±0.23	0.00	0.01±0.04	0.00
<i>n</i> -Hexane	0.84±0.14	0.00	0.12±0.13	0.05	0.04±0.05	0.03
2,2-Dimethylbutane	0.32±0.55	0.00	0.03±0.06	0.01	0.02±0.03	0.00
2-Methylpentane	0.33±0.62	0.00	0.10±0.15	0.01	0.04±0.09	0.00
3-Methylpentane	0.31±0.77	0.00	0.07±0.09	0.03	0.04±0.07	0.01
4-Methyl-1-pentene	0.07±0.15	0.00	0.08±0.07	0.06	0.02±0.02	0.00
Benzene	16.63±25.41	5.51	0.88±0.59	0.79	0.28±0.24	0.19
<i>n</i> -Heptane	1.13±1.58	0.00	0.06±0.06	0.04	0.02±0.03	0.01
2,3-Dimethylpentane	0.45±1.12	0.00	0.16±0.31	0.03	0.09±0.16	0.01
2,4-Dimethylpentane	0.11±0.17	0.00	0.16±0.32	0.08	0.16±0.19	0.07
2-Methylhexane	0.37±0.84	0.00	0.04±0.04	0.00	0.02±0.04	0.00
Toluene	7.31±18.14	0.00	0.54±0.59	0.27	0.19±0.20	0.08
<i>n</i> -Octane	0.75±1.05	0.00	0.04±0.07	0.00	0.00±0.01	0.00
2,2,4-Trimethylpentane	0.11±0.17	0.00	0.05±0.15	0.00	0.10±0.29	0.00
2,3,4-Trimethylpentane	0.08±0.13	0.00	0.06±0.20	0.00	0.07±0.18	0.00
<i>m,p</i> -Xylene	2.23±3.44	0.03	0.14±0.20	0.00	0.10±0.15	0.02
Ethylbenzene	1.87±2.47	0.59	0.08±0.08	0.04	0.03±0.04	0.01
<i>n</i> -Nonane	0.13±0.45	0.00	0.05±0.11	0.00	0.09±0.38	0.00
1,2,4-Trimethylbenzene	1.46±1.96	0.11	0.05±0.05	0.04	0.05±0.08	0.02
Total alkanes	15.0±7.7	14.2	2.7±2.3	1.7	1.8±1.9	1.0
Total alkenes	8.1±7.6	6.0	1.0±0.9	0.8	0.5±0.6	0.2
Total aromatics	32.0±40.5	15.7	1.8±1.4	1.5	0.8±0.8	0.4
Total NMHCs	55.1±45.7	34.5	5.5±4.4	3.7	3.1±3.1	1.6

Units are ppbv except for specified parameters.

## The IPAC-NC field campaign

J. Z. Ma et al.

**Table 4.** OH budget at different altitudes based on a model analysis of measurement data with and without considering heterogeneous reactions (HR) of OH and HO<sub>2</sub> on aerosol surfaces.

Item	Surface		0.8 km		1.6 km		2.4 km	
	HR	NO_HR	HR	NO_HR	HR	NO_HR	HR	NO_HR
Production (molecules cm <sup>-3</sup> s <sup>-1</sup> )	2.4 × 10 <sup>8</sup>	2.5 × 10 <sup>8</sup>	8.3 × 10 <sup>7</sup>	1.0 × 10 <sup>8</sup>	3.9 × 10 <sup>7</sup>	4.3 × 10 <sup>7</sup>	2.2 × 10 <sup>7</sup>	2.3 × 10 <sup>7</sup>
NO + HO <sub>2</sub>	<b>93 %</b>	<b>93 %</b>	<b>91 %</b>	<b>92 %</b>	<b>88 %</b>	<b>89 %</b>	<b>87 %</b>	<b>87 %</b>
HNO <sub>2</sub> + hν	2 %	2 %	2 %	2 %	2 %	2 %	3 %	3 %
H <sub>2</sub> O + O( <sup>1</sup> D)	2 %	2 %	<b>6 %</b>	<b>5 %</b>	<b>7 %</b>	<b>6 %</b>	<b>7 %</b>	<b>7 %</b>
[CH <sub>3</sub> CHOO] <sup>+</sup>	1 %	1 %	<1 %	<1 %	<1 %	<1 %	<1 %	<1 %
H <sub>2</sub> O + CH <sub>3</sub> CH(OO.)	1 %	1 %	<1 %	<1 %	<1 %	<1 %	<1 %	<1 %
H <sub>2</sub> O <sub>2</sub> + hν	<1 %	<1 %	<1 %	<1 %	1 %	1 %	1 %	1 %
remaining	<1 %	<1 %	<1 %	<1 %	<2 %	<2 %	<2 %	<2 %
Loss (molecules cm <sup>-3</sup> s <sup>-1</sup> )	2.4 × 10 <sup>8</sup>	2.5 × 10 <sup>8</sup>	8.3 × 10 <sup>7</sup>	1.0 × 10 <sup>8</sup>	3.9 × 10 <sup>7</sup>	4.3 × 10 <sup>7</sup>	2.2 × 10 <sup>7</sup>	2.3 × 10 <sup>7</sup>
CO + OH	<b>21 %</b>	<b>21 %</b>	<b>33 %</b>	<b>33 %</b>	<b>17 %</b>	<b>17 %</b>	<b>15 %</b>	<b>15 %</b>
NO <sub>2</sub> + OH	<b>18 %</b>	<b>18 %</b>	<b>14 %</b>	<b>14 %</b>	<b>17 %</b>	<b>17 %</b>	<b>21 %</b>	<b>21 %</b>
C <sub>6</sub> H <sub>4</sub> CH <sub>3</sub> + CH <sub>3</sub> + OH	<b>8 %</b>	<b>8 %</b>	1 %	1 %	2 %	2 %	2 %	2 %
CH <sub>3</sub> CH=CHCH <sub>3</sub> + OH	<b>8 %</b>	<b>8 %</b>	1 %	1 %	<1 %	<1 %	<1 %	<1 %
(CH <sub>3</sub> ) <sub>2</sub> C=CH <sub>2</sub> + OH	6 %	6 %	6 %	6 %	5 %	5 %	5 %	5 %
CH <sub>3</sub> CHO + OH	5 %	5 %	4 %	4 %	3 %	3 %	2 %	2 %
C <sub>6</sub> H <sub>5</sub> CH <sub>3</sub> + OH	3 %	3 %	1 %	1 %	<1 %	<1 %	<1 %	<1 %
SO <sub>2</sub> + OH	3 %	3 %	<b>16 %</b>	<b>16 %</b>	<b>15 %</b>	<b>15 %</b>	<b>16 %</b>	<b>16 %</b>
CH <sub>2</sub> O + OH	3 %	3 %	6 %	6 %	6 %	6 %	5 %	5 %
C <sub>3</sub> H <sub>6</sub> + OH	3 %	3 %	2 %	2 %	2 %	2 %	2 %	2 %
CHOCH=C(CH <sub>3</sub> )CHO + OH	3 %	3 %	<1 %	<1 %	<1 %	<1 %	<1 %	<1 %
NO + OH	3 %	2 %	2 %	2 %	2 %	2 %	3 %	3 %
CH <sub>4</sub> + OH	<2 %	<2 %	2 %	2 %	2 %	2 %	3 %	3 %
C <sub>9</sub> H <sub>13</sub> CH <sub>3</sub> + OH	<2 %	<2 %	<2 %	<2 %	7 %	7 %	6 %	6 %
dtA1 + OH	<2 %	<2 %	<2 %	<2 %	6 %	6 %	5 %	5 %
remaining	<16 %	<17 %	<12 %	<12 %	<16 %	<16 %	<15 %	<15 %
Concentration (molecules cm <sup>-3</sup> )	5.4 × 10 <sup>6</sup>	5.7 × 10 <sup>6</sup>	6.9 × 10 <sup>6</sup>	8.5 × 10 <sup>6</sup>	4.7 × 10 <sup>6</sup>	5.2 × 10 <sup>6</sup>	3.8 × 10 <sup>6</sup>	4.1 × 10 <sup>6</sup>

dtA1: CH<sub>3</sub>CO'CH'CH<sub>2</sub>'CH(CH<sub>2</sub>CHO)'CCH<sub>3</sub>CH<sub>3</sub>.

Title Page

Abstract

Introduction

Conclusions

References

Tables

Figures

◀

▶

◀

▶

Back

Close

Full Screen / Esc

Printer-friendly Version

Interactive Discussion



**Table 5.** HO<sub>2</sub> budget at different altitudes based on a model analysis of measurement data with and without considering heterogeneous reactions (HR) of OH and HO<sub>2</sub> on aerosol surfaces.

Item	Surface		0.8 km		1.6 km		2.4 km	
	HR	NO_HR	HR	NO_HR	HR	NO_HR	HR	NO_HR
Production (molecules cm <sup>-3</sup> s <sup>-1</sup> )	2.2 × 10 <sup>8</sup>	2.3 × 10 <sup>8</sup>	8.0 × 10 <sup>7</sup>	9.7 × 10 <sup>8</sup>	3.6 × 10 <sup>7</sup>	3.8 × 10 <sup>7</sup>	1.9 × 10 <sup>7</sup>	2.0 × 10 <sup>7</sup>
CO + OH	<b>22%</b>	<b>22%</b>	<b>34%</b>	<b>35%</b>	<b>19%</b>	<b>19%</b>	<b>17%</b>	<b>17%</b>
CH <sub>3</sub> O + O <sub>2</sub>	<b>9%</b>	<b>9%</b>	<b>8%</b>	<b>8%</b>	<b>8%</b>	<b>8%</b>	<b>8%</b>	<b>8%</b>
CH <sub>3</sub> CH(OH)CH(O.)CH <sub>3</sub>	<b>8%</b>	<b>8%</b>	1%	1%	< 1%	< 1%	< 1%	< 1%
C <sub>6</sub> H <sub>3</sub> CH <sub>3</sub> , HOH, CH <sub>3</sub> /(OO.) + NO	<b>7%</b>	<b>7%</b>	1%	1%	2%	2%	2%	2%
CH <sub>3</sub> COCH=CHCHO + hv	4%	4%	1%	1%	1%	1%	1%	1%
CH <sub>2</sub> O + hv	4%	4%	<b>9%</b>	<b>7%</b>	<b>13%</b>	<b>12%</b>	<b>16%</b>	<b>15%</b>
CH <sub>3</sub> COCH(O.)CHO + O <sub>2</sub>	4%	4%	1%	1%	1%	1%	1%	1%
CH <sub>2</sub> O + OH	3%	3%	7%	7%	6%	6%	6%	6%
SO <sub>2</sub> + OH	3%	3%	<b>17%</b>	<b>17%</b>	<b>16%</b>	<b>17%</b>	<b>18%</b>	<b>18%</b>
CH <sub>3</sub> C(OH)(CH <sub>3</sub> )CH <sub>2</sub> (O.)	3%	3%	3%	3%	3%	3%	2%	2%
CH <sub>2</sub> (OH)C(O.)(CH <sub>3</sub> )CH <sub>3</sub>	3%	3%	3%	3%	3%	3%	2%	2%
CH <sub>2</sub> (OH)(OO.)	2%	2%	2%	2%	2%	2%	2%	2%
CH <sub>3</sub> COCHO + hv	2%	2%	1%	1%	2%	2%	2%	2%
[CH <sub>3</sub> CHOO]*	2%	2%	< 1%	< 1%	< 1%	< 1%	< 1%	< 1%
C <sub>9</sub> H <sub>12</sub> CH <sub>3</sub> , (O.), HOH	< 2%	< 2%	< 2%	< 2%	7%	7%	7%	7%
remaining	<b>&lt; 24%</b>	<b>&lt; 24%</b>	<b>&lt; 12%</b>	<b>&lt; 13%</b>	<b>&lt; 17%</b>	<b>&lt; 17%</b>	<b>&lt; 16%</b>	<b>&lt; 17%</b>
Loss (molecules cm <sup>-3</sup> s <sup>-1</sup> )	2.2 × 10 <sup>8</sup>	2.3 × 10 <sup>8</sup>	8.0 × 10 <sup>7</sup>	9.7 × 10 <sup>8</sup>	3.6 × 10 <sup>7</sup>	3.8 × 10 <sup>7</sup>	1.9 × 10 <sup>7</sup>	2.0 × 10 <sup>7</sup>
NO + HO <sub>2</sub>	<b>98%</b>	<b>99%</b>	<b>94%</b>	<b>98%</b>	<b>95%</b>	<b>98%</b>	<b>96%</b>	<b>98%</b>
HO <sub>2</sub> + surface	1%	–	4%	–	3%	–	2%	–
CH <sub>2</sub> O + HO <sub>2</sub>	< 1%	< 1%	1%	1%	1%	1%	1%	1%
O <sub>3</sub> + HO <sub>2</sub>	< 1%	< 1%	< 1%	< 1%	1%	1%	1%	1%
HO <sub>2</sub> + HO <sub>2</sub>	< 1%	< 1%	< 1%	1%	< 1%	< 1%	< 1%	< 1%
remaining	< 1%	< 1%	< 1%	< 1%	< 1%	< 1%	< 1%	< 1%
Concentration (molecules cm <sup>-3</sup> )	1.2 × 10 <sup>8</sup>	1.3 × 10 <sup>8</sup>	1.8 × 10 <sup>8</sup>	2.3 × 10 <sup>8</sup>	1.0 × 10 <sup>8</sup>	1.1 × 10 <sup>8</sup>	6.3 × 10 <sup>7</sup>	6.7 × 10 <sup>7</sup>

## The IPAC-NC field campaign

J. Z. Ma et al.

Title Page

Abstract

Introduction

Conclusions

References

Tables

Figures

◀

▶

◀

▶

Back

Close

Full Screen / Esc

Printer-friendly Version

Interactive Discussion



## The IPAC-NC field campaign

J. Z. Ma et al.

**Table 6.** Ozone budget at different altitudes based on a model analysis of measurement data with and without considering heterogeneous reactions (HR) of OH and HO<sub>2</sub> on aerosol surfaces.

Item	Surface		0.8 km		1.6 km		2.4 km	
	HR	NO_HR	HR	NO_HR	HR	NO_HR	HR	NO_HR
Production (ppbv hr <sup>-1</sup> )	48.3	51.6	15.5	19.6	8.4	9.3	4.9	5.3
NO + HO <sub>2</sub>	<b>65%</b>	<b>65%</b>	<b>74%</b>	<b>75%</b>	<b>67%</b>	<b>68%</b>	<b>70%</b>	<b>70%</b>
CH <sub>3</sub> (OO.) + NO	6%	6%	6%	6%	6%	5%	6%	6%
CH <sub>3</sub> CH(OH)CH(OO.)CH <sub>3</sub> + NO	5%	5%	1%	1%	< 1%	< 1%	< 1%	< 1%
CH <sub>3</sub> CO(OO.) + NO	3%	3%	4%	4%	3%	3%	2%	2%
C <sub>6</sub> H <sub>5</sub> CH <sub>2</sub> OH, CH <sub>3</sub> /(OO.) + NO	2%	2%	1%	1%	1%	1%	1%	1%
CH <sub>3</sub> C(OO.)(CH <sub>3</sub> )CH <sub>2</sub> (OH) + NO	2%	2%	2%	2%	2%	2%	2%	2%
CH <sub>3</sub> C(OH)(CH <sub>3</sub> )CH <sub>2</sub> (OO.) + NO	2%	2%	2%	2%	2%	2%	2%	2%
CH <sub>3</sub> COCH=CHCO(OO.) + NO	2%	2%	1%	1%	< 1%	< 1%	1%	1%
C <sub>9</sub> H <sub>12</sub> (CH <sub>3</sub> )(OO.)H(OH) + NO	1%	1%	< 1%	< 1%	5%	5%	5%	5%
2t91 + NO	< 1%	< 1%	< 1%	< 1%	2%	2%	2%	2%
remaining	< 12%	< 12%	< 9%	< 8%	< 12%	< 12%	< 9%	< 9%
Loss (ppbv hr <sup>-1</sup> )	8.5	9.1	2.8	3.2	1.7	1.9	1.2	1.3
NO <sub>2</sub> + OH	<b>69%</b>	<b>70%</b>	<b>66%</b>	<b>70%</b>	<b>62%</b>	<b>63%</b>	<b>68%</b>	<b>69%</b>
CH <sub>3</sub> CH=CHCH <sub>3</sub> + O <sub>3</sub>	<b>16%</b>	<b>15%</b>	1%	1%	< 1%	< 1%	< 1%	< 1%
O <sub>3</sub> + surface	<b>8%</b>	<b>7%</b>	<b>15%</b>	<b>13%</b>	<b>14%</b>	<b>13%</b>	<b>10%</b>	<b>10%</b>
H <sub>2</sub> O + O( <sup>1</sup> D)	3%	3%	<b>13%</b>	<b>12%</b>	<b>13%</b>	<b>12%</b>	<b>11%</b>	<b>11%</b>
C <sub>9</sub> H <sub>13</sub> CH <sub>3</sub> + O <sub>3</sub>	1%	1%	< 1%	< 1%	6%	6%	5%	5%
O <sub>3</sub> + HO	1%	1%	2%	2%	2%	2%	2%	3%
O <sub>3</sub> + HO <sub>2</sub>	1%	1%	2%	1%	2%	2%	1%	1%
remaining	< 1%	< 2%	< 1%	< 1%	< 1%	< 2%	< 3%	< 1%
Net production (ppbv hr <sup>-1</sup> )	39.7	42.5	12.7	16.3	6.7	7.4	3.7	4.0

2t91: CH<sub>3</sub>CO'CH'CH<sub>2</sub>CH(CH<sub>2</sub>OO.)'CCH<sub>3</sub>CH<sub>3</sub>.

Title Page

Abstract

Introduction

Conclusions

References

Tables

Figures

◀

▶

◀

▶

Back

Close

Full Screen / Esc

Printer-friendly Version

Interactive Discussion



**The IPAC-NC field campaign**

J. Z. Ma et al.

Title Page

Abstract

Introduction

Conclusions

References

Tables

Figures

◀

▶

◀

▶

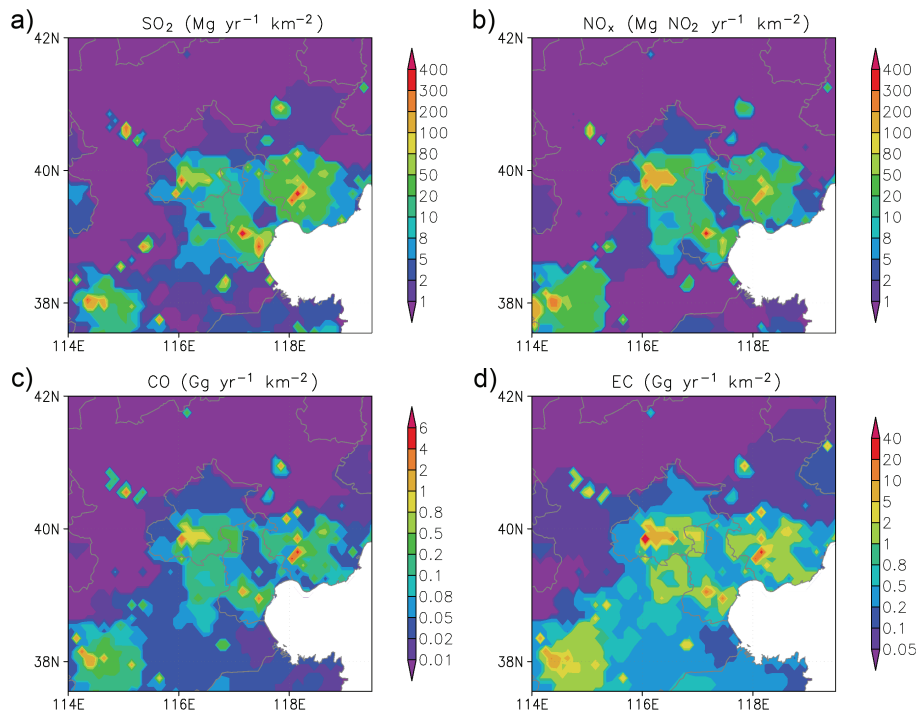
Back

Close

Full Screen / Esc

Printer-friendly Version

Interactive Discussion

**Fig. 1.** Primary pollutant emissions in the central area of Huabei.

## The IPAC-NC field campaign

J. Z. Ma et al.

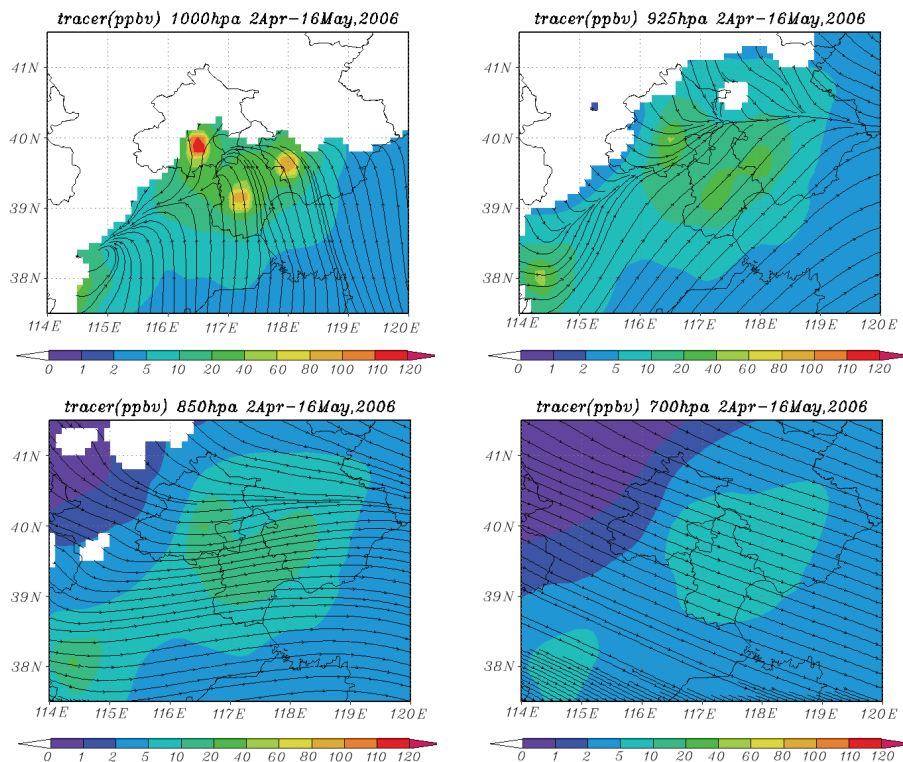


**Fig. 2.** Model simulated wind fields and spatial distributions of pollution tracers emitted from major urban centers of Huabei. Mountain areas are masked by blanks. The model predicts an air pollution pool over the Jing-Jin-Tang area.

Title Page

Abstract

Introduction

Conclusions

References

Tables

Figures

◀

▶

◀

▶

Back

Close

Full Screen / Esc

Printer-friendly Version

Interactive Discussion



## The IPAC-NC field campaign

J. Z. Ma et al.

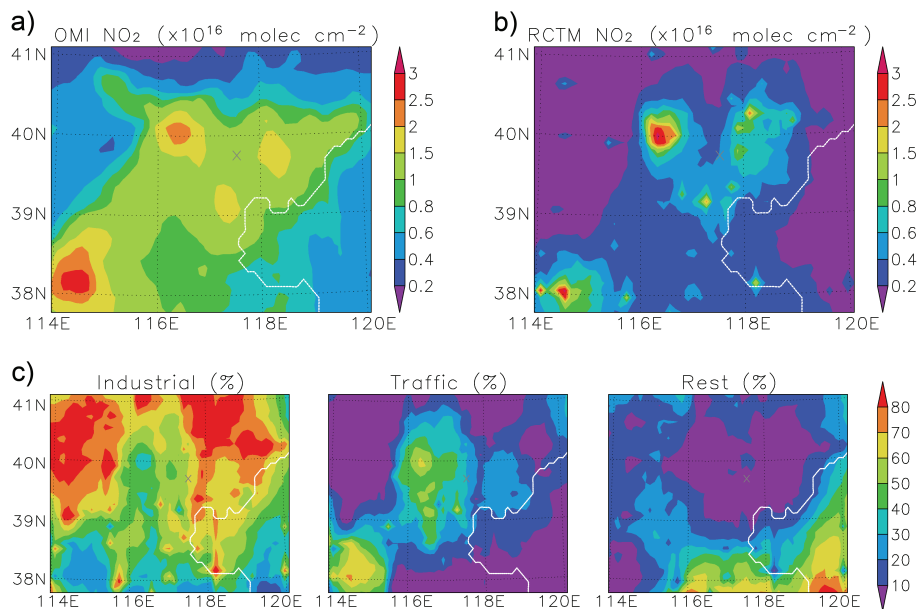


**Fig. 3.** Vertical column densities of tropospheric NO<sub>2</sub> during IPAC-NC. **(a)** OMI satellite data. **(b)** RCTM simulated results. **(c)** Percentage contributions from industrial, traffic, and other sources estimated with a tracer-tagging method. Industrial emissions predominantly contribute to the air pollution pool.

[Title Page](#)[Abstract](#)[Introduction](#)[Conclusions](#)[References](#)[Tables](#)[Figures](#)[◀](#)[▶](#)[◀](#)[▶](#)[Back](#)[Close](#)[Full Screen / Esc](#)[Printer-friendly Version](#)[Interactive Discussion](#)

## The IPAC-NC field campaign

J. Z. Ma et al.

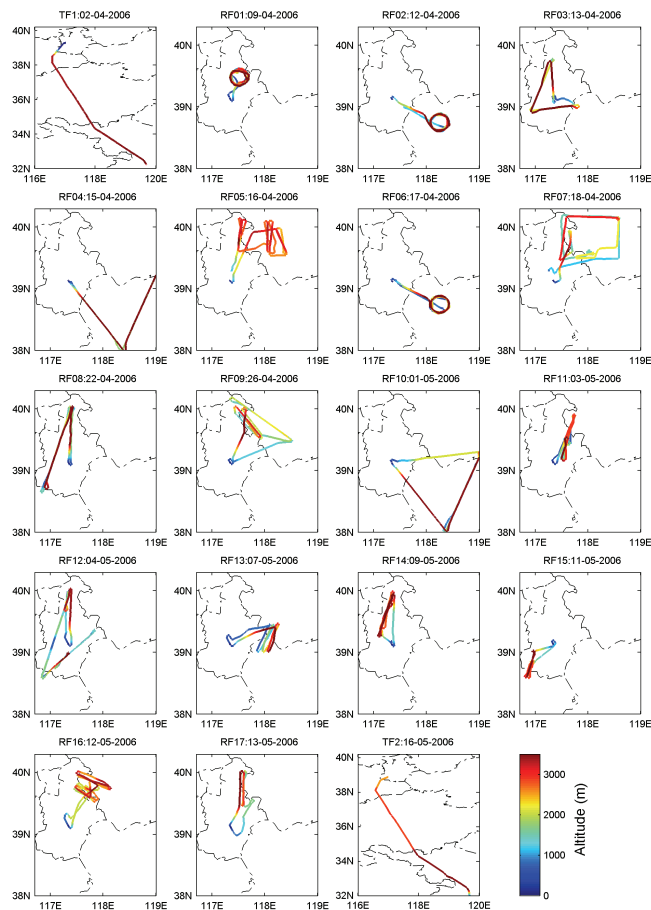


**Fig. 4.** YUN-12 individual flight tracks during IPAC-NC colored by altitude. Two transfer flights and 17 research flights were performed from 2 April to 16 May 2006.

[Title Page](#)[Abstract](#)[Introduction](#)[Conclusions](#)[References](#)[Tables](#)[Figures](#)[◀](#)[▶](#)[◀](#)[▶](#)[Back](#)[Close](#)[Full Screen / Esc](#)[Printer-friendly Version](#)[Interactive Discussion](#)

**The IPAC-NC field campaign**

J. Z. Ma et al.

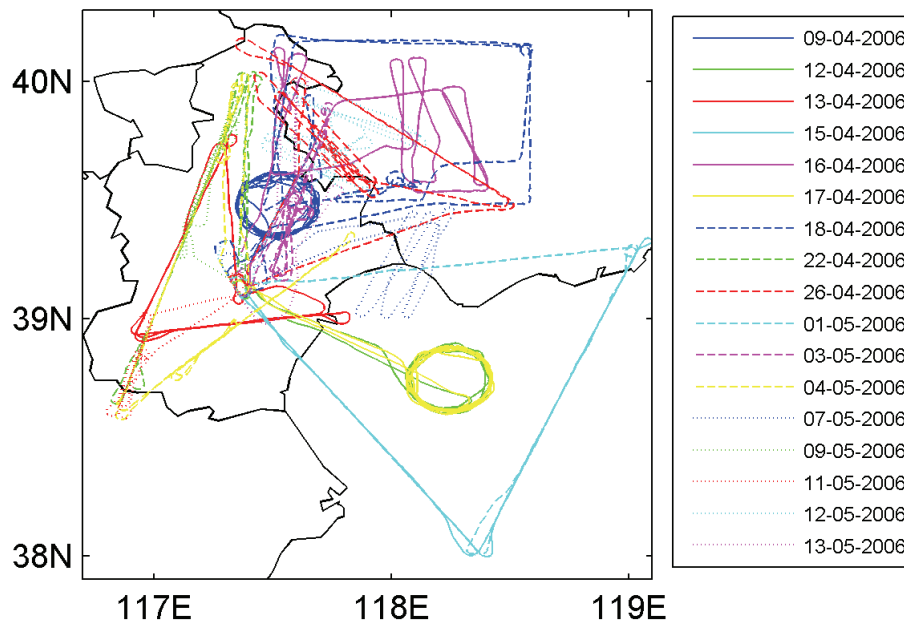


**Fig. 5.** Superposition of 17 research flight tracks during IPAC-NC. Majority of flights were performed within the core area of the air pollution pool.

[Title Page](#)[Abstract](#)[Introduction](#)[Conclusions](#)[References](#)[Tables](#)[Figures](#)[◀](#)[▶](#)[◀](#)[▶](#)[Back](#)[Close](#)[Full Screen / Esc](#)[Printer-friendly Version](#)[Interactive Discussion](#)

## The IPAC-NC field campaign

J. Z. Ma et al.

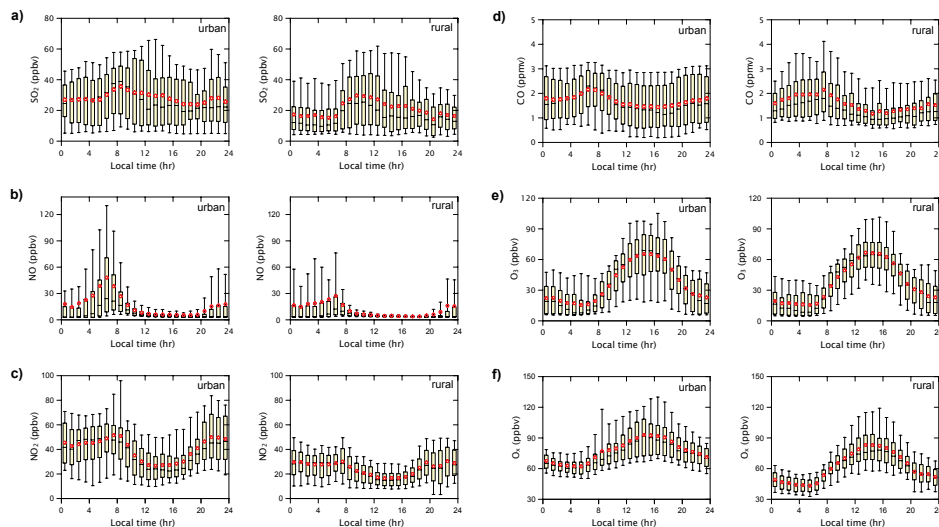


**Fig. 6.** Diurnal cycles of **(a)**  $\text{SO}_2$ , **(b)**  $\text{NO}$ , **(c)**  $\text{NO}_2$ , **(d)**  $\text{CO}$ , **(e)**  $\text{O}_3$ , and **(f)**  $\text{O}_x$  at the Beigongda (urban) and Xin'an (rural) sites during IPAC-NC. Lower (upper) error bars and yellow boxes are 10th (90th) and 25th (75th) percentiles of the data grouped in one-hour intervals, respectively. Hyphens inside the boxes are the medians and red circles the mean values.

Title Page

Abstract

Introduction

Conclusions

References

Tables

Figures

◀

▶

◀

▶

Back

Close

Full Screen / Esc

Printer-friendly Version

Interactive Discussion



## The IPAC-NC field campaign

J. Z. Ma et al.

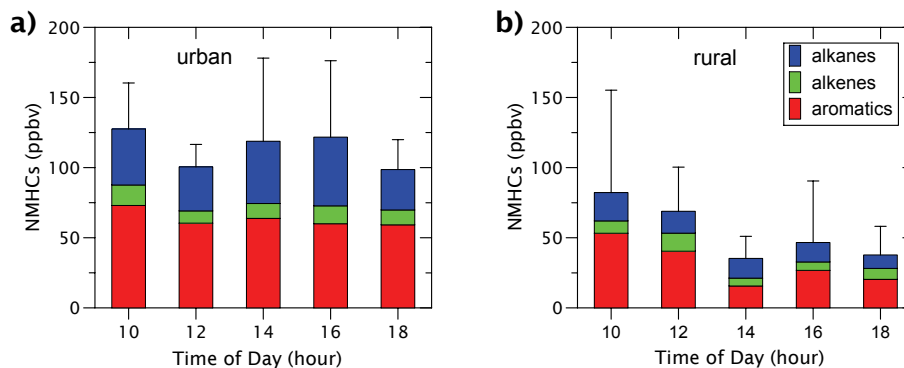


**Fig. 7.** Diel variations of alkanes, alkenes and aromatics as a function of local standard time as measured at **(a)** the Beigongda (urban) site and **(b)** the Xin'an (rural) site during IPAC-NC. Error bars are standard deviations of total NMHCs in the upper direction.

[Title Page](#)[Abstract](#)[Introduction](#)[Conclusions](#)[References](#)[Tables](#)[Figures](#)[◀](#)[▶](#)[◀](#)[▶](#)[Back](#)[Close](#)[Full Screen / Esc](#)[Printer-friendly Version](#)[Interactive Discussion](#)

## The IPAC-NC field campaign

J. Z. Ma et al.

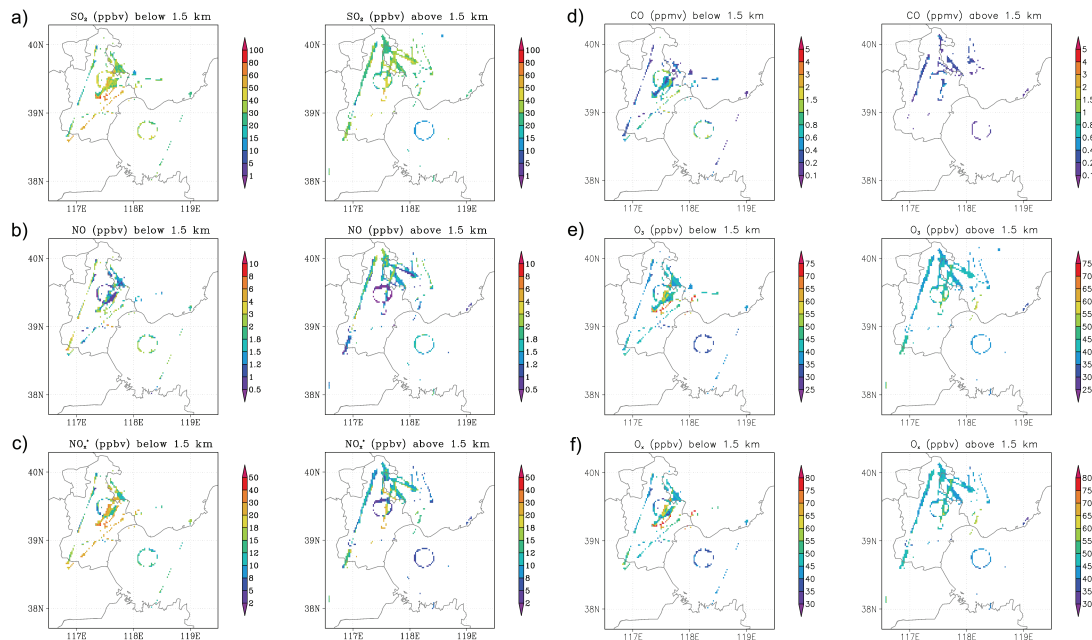


**Fig. 8.** Flight track of all data collected from the aircraft below (left) and above (right) 1.5 km colored by (a)  $\text{SO}_2$ , (b) NO, (c)  $\text{NO}_x^*$ , (d) CO, (e)  $\text{O}_3$ , and (f)  $\text{O}_x$  mixing ratios during IPAC-NC.

Title Page

Abstract

Introduction

Conclusions

References

Tables

Figures

◀

▶

◀

▶

Back

Close

Full Screen / Esc

Printer-friendly Version

Interactive Discussion



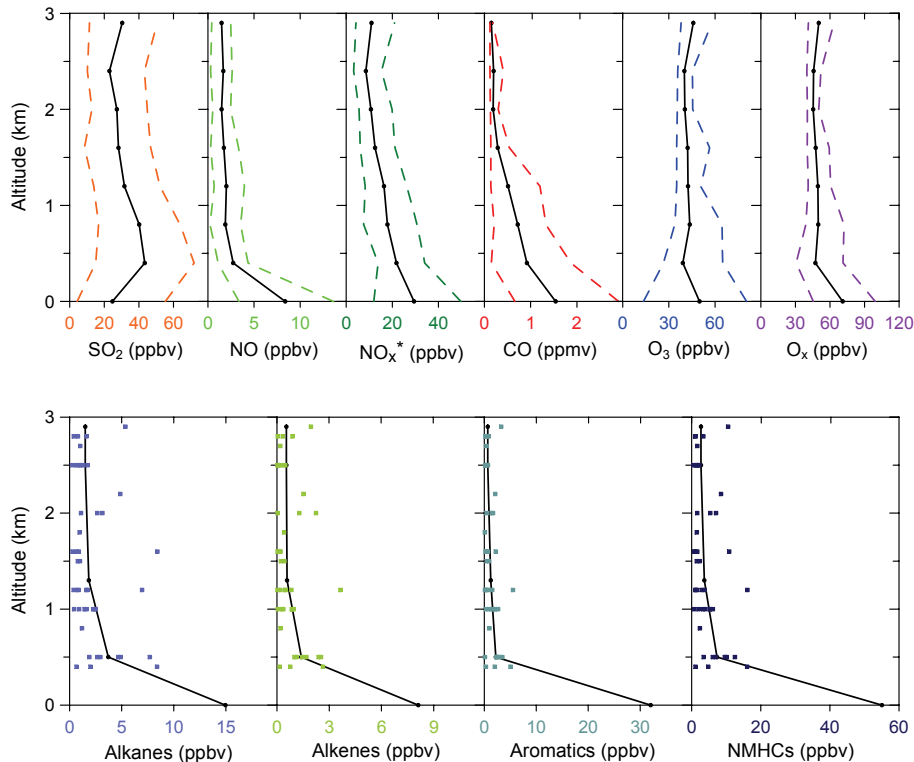


**Fig. 9.** Vertical profiles of gaseous pollutants measured by aircraft combined with daytime surface measurements at the Xin'an station. Black solid lines are mean values, colored dashed lines are 10th and 90th percentiles of the data for inorganic gases, and colored dots are values for each VOC sample. O<sub>x</sub> is O<sub>3</sub> plus NO<sub>2</sub>, the latter derived by scaling measured NO with the NO<sub>2</sub>/NO ratios simulated with our RCTM.

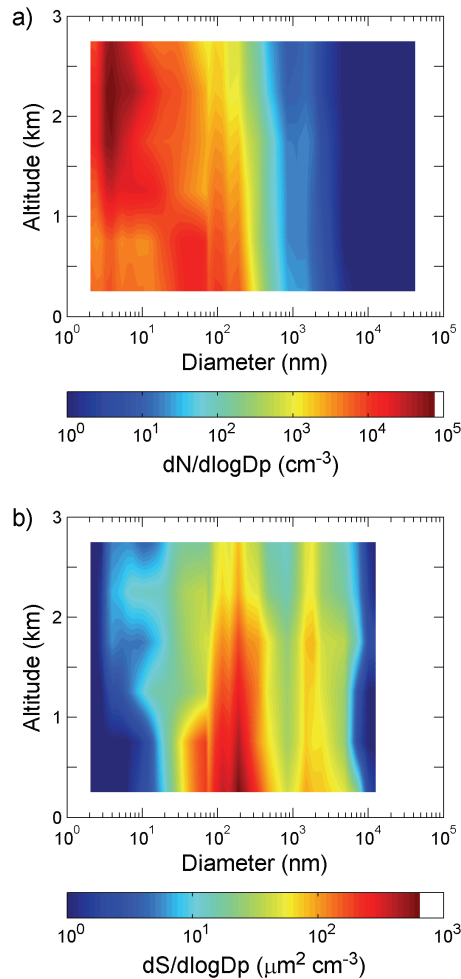


**Fig. 10.** Size distributions of **(a)** aerosol number and **(b)** surface area as a function of altitude, measured by aircraft.

27760

**The IPAC-NC field campaign**

J. Z. Ma et al.

Title Page	
Abstract	Introduction
Conclusions	References
Tables	Figures
◀	▶
◀	▶
Back	Close
Full Screen / Esc	
Printer-friendly Version	
Interactive Discussion	



## The IPAC-NC field campaign

J. Z. Ma et al.

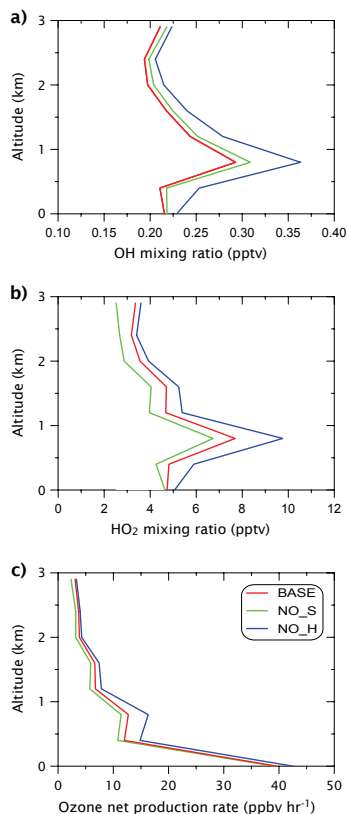


**Fig. 11.** Vertical profiles of (a) OH, (b) HO<sub>2</sub>, and (c) O<sub>3</sub> production rates, calculated using the NCAR Master Mechanism constrained by measured daytime mean trace gas and aerosol concentrations. BASE refers to the standard simulation, and NO\_S and NO\_H to sensitivity simulations without considering SO<sub>2</sub> related reactions and heterogeneous reactions of OH and HO<sub>2</sub> on aerosol surfaces, respectively.

[Title Page](#)[Abstract](#)[Introduction](#)[Conclusions](#)[References](#)[Tables](#)[Figures](#)[◀](#)[▶](#)[◀](#)[▶](#)[Back](#)[Close](#)[Full Screen / Esc](#)[Printer-friendly Version](#)[Interactive Discussion](#)

## The IPAC-NC field campaign

J. Z. Ma et al.

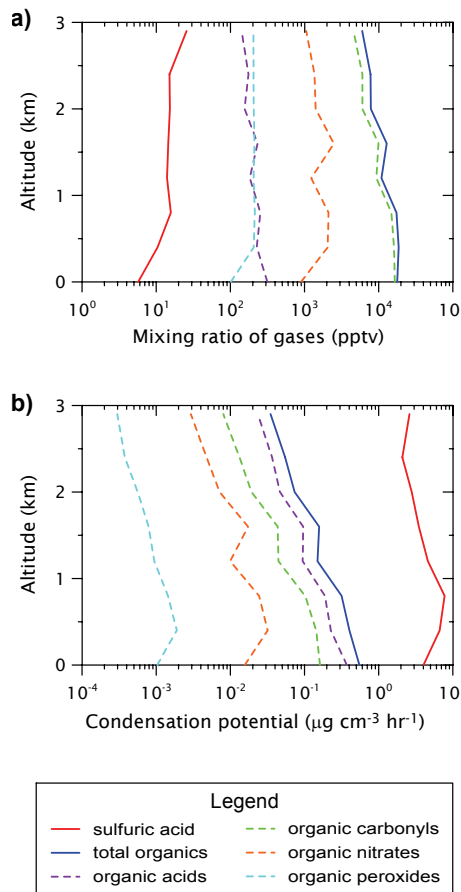


**Fig. 12.** Vertical profiles of (a) sulfuric acid and VOC oxidation products and (b) their condensation potential on aerosol surfaces calculated using the NCAR Master Mechanism constrained by measured daytime mean trace gas and aerosol concentrations.